

Gravitational wave emission and spindown of young pulsars

Mark G. Alford and Kai Schwenzer

Department of Physics, Washington University, St. Louis, Missouri, 63130, USA

The rotation frequencies of young pulsars are systematically below their theoretical Kepler limit. R-modes have been suggested as a possible explanation for this observation. With the help of semi-analytic expressions that make it possible to assess the uncertainties of the r-mode scenario due to the impact of uncertainties in underlying microphysics, we perform a quantitative analysis of the the spin-down and the emitted gravitational waves of young pulsars. We find that the frequency to which r-modes spin down a young neutron star as well as the characteristic gravitational wave strain amplitude are extremely insensitive both to the microscopic details and the saturation amplitude. Comparing our result to astrophysical data, we show that for a range of saturation amplitudes r-modes provide a viable spindown scenario and that all observed young pulsars are very likely already outside the r-mode instability region. Taking into account the finite observation time, we find that the signal to noise ratio for gravitational waves is smaller than previous estimates, but large enough to detect such sources with next generation detectors.

I. INTRODUCTION

A neutron star is a complex system whose behavior is influenced by physics on scales from the Fermi scale to its size and whose description involves all forces of nature. This holds in particular when dynamical aspects involving mechanical oscillations coupled to radiation fields are considered and a description should thereby intricately depend on all these details. Yet, the surprising finding presented in this work is that for some of the most relevant observables analytic expressions can be derived that are strikingly insensitive to these complicated microscopic as well as macroscopic details.

The rotation frequencies of pulsars, as well as their time derivatives, are among the most precise observations in physics. These frequencies change over time due to magnetic braking and other possible spindown mechanisms like gravitational wave emission due to deformations or oscillation modes of the star. In particular the unstable r-modes [1, 2] are interesting because they must be stabilized by a viscous dissipation mechanism and thereby can probe the microphysics deep inside the star. It has already been shown [3, 4] that important aspects of the instability regions of r-modes are very insensitive to quantitative microscopic details but do depend on qualitative differences of the various possible forms of dense matter. Here we extend this study to the dynamical r-mode evolution of neutron stars and show that in this case the insensitivity to unknown input parameters is even more pronounced. In particular we derive semi-analytic expressions for the final frequency of the spin-down evolution and the spindown time of young neutron stars and show that these quantities are likewise insensitive to the particular r-mode saturation mechanism.

Magnetic dipole radiation is considered as a standard mechanism for the spindown of pulsars and is used to determine an approximate characteristic spindown age [5]. In contrast, in this work we will instead only consider the spindown torque due to r-modes, which is only non-vanishing as long as the star is within the unstable

region. Our results therefore provide upper limits on the actual frequencies of observed pulsars and should apply as long as the r-mode spindown dominates. However, they might not be applicable to magnetars where this is not guaranteed. A more detailed analysis which includes both electromagnetic and gravitational radiation [6] and thereby allows to make contact to pulsar ages will be given elsewhere.

The fastest young pulsar observed so far is PSR J0537-6910 with a rotational frequency of $f \approx 62$ Hz, which has been associated to the remnant N157B of a supernova that exploded in the Large Magellanic Cloud [7]. We find that this spin frequency is just below the final frequency due to pure r-mode emission of a neutron star with standard modified Urca beta equilibration processes, so that r-mode emission could indeed provide a quantitative explanation for the low spin frequencies of young neutron stars. If the r-mode scenario is realized, the fact that all observed stars are below the r-mode bound also suggests that r-mode spindown should be fast, i.e. at least comparable to magnetic spindown, which would require a high r-mode saturation amplitude $\alpha \gtrsim 0.01$ in young neutron stars.

R-modes are an important source of gravitational waves and provide an interesting possibility for their detection since r-modes can radiate over long times. Previously analytic estimates have been given for the gravitational wave strain of r-modes of young stars [8]. As found in the latter work the most important quantity for the detectability of the gravitational wave signal is the minimum frequency emitted during the evolution. Here we extend this analysis and our semi-analytic results allow us to determine the minimum gravitational strain expected from r-modes as well as the signal to noise ratio for their detection in forthcoming second generation detectors like advanced LIGO [9, 10]. Furthermore we point out that the limited observation time can strongly reduce the detectability of such sources.

II. MATERIAL AND STAR PROPERTIES

As noted before a neutron star is a complex system and the description of its spindown evolution requires an understanding of various different aspects. The starting point is the static star configuration which is determined by gravity as described by the general relativistic Tolman-Oppenheimer-Volkov (TOV) equations [11]. The latter require the equation of state of charge-neutral dense matter in beta equilibrium as an ingredient which is determined by microscopic strong interactions. Both the rotation and the oscillation of the star are modeled as perturbations of the static respectively the rotating star configuration [12]. For simplicity both are standardly obtained from the Newtonian Euler-equation of a non-viscous fluid. The classical r-modes with $l = m$ are given by the Eulerian velocity perturbations

$$\delta \vec{v} = \alpha R \Omega \left(\frac{r}{R} \right)^m \vec{Y}_{mm}^B(\theta, \varphi) e^{i\omega t}, \quad (1)$$

where α is a dimensionless amplitude parameter, R is the star radius, Ω and ω are rotational and mode angular velocity, respectively, and \vec{Y}^B is the magnetic vector spherical harmonic with magnetic quantum number m .

To describe the dynamical evolution requires microscopic material properties of the dense matter within the star. Here we follow the method that was developed previously in [3] and [4] to obtain semi-analytic results for the boundary of the r-mode instability region as well as for the saturation amplitude in case suprathermal bulk viscosity saturates the mode. The basic idea is that the microscopic material properties that are relevant for the pulsar evolution have - at least over the range required to describe the relevant aspects - simple power law dependencies on the temperature T , the oscillation frequency ω and the density oscillation amplitude $\Delta n / \bar{n}$. The required quantities for the star evolution are the shear viscosity η , the bulk viscosity ζ , the specific heat c_V and the neutrino emissivity ϵ . Both the the bulk viscosity and the neutrino emissivity are determined by a weak equilibration process whose rate in a degenerate system has the form $\Gamma^{(\leftrightarrow)} = -\tilde{\Gamma} T^\delta \mu_\Delta$, where μ_Δ is the chemical potential difference that is driven out of equilibrium. Here we neglect the suprathermal amplitude dependence of the bulk viscosity and the neutrino emissivity [13, 14] and leave this for future work. In the subthermal regime these quantities can generally be parameterized as

$$\eta = \tilde{\eta} T^{-\sigma}, \quad \zeta \approx \frac{C^2 \tilde{\Gamma} T^\delta}{\omega^2 + (B \tilde{\Gamma} T^\delta)^2} \rightarrow \frac{C^2 \tilde{\Gamma} T^\delta}{\omega^2}, \quad (2)$$

$$c_V = \tilde{c}_V T^v, \quad \epsilon \approx \tilde{\epsilon} T^\theta, \quad (3)$$

where B and C are non-equilibrium susceptibilities. With such power law behavior it is clear that physical results should depend far more sensitively on the exponents σ , δ , v and θ than on the prefactor functions $\tilde{\eta}$,

\tilde{c}_V , $\tilde{\epsilon}$, \dots . The important point is that the exponents are the same for a given phase of dense matter, like e.g. hadronic matter with modified Urca reactions, and quantitative details due to the unknown equation of state or the interactions are only reflected in the prefactors. Strikingly we will see below that the quantitative dependence on these prefactors can be even far more insensitive than this general argument suggests. Different phases of dense matter, however, can feature qualitatively different low energy degrees of freedom resulting in different exponents and thereby can lead to a qualitatively very different star evolution.

The above material properties are local quantities, but all that enters the evolution equations below are quantities that are averaged over the entire star. These are the power radiated in gravitational waves P_G , the dissipated power P_S and P_B due to shear and bulk viscosity, the specific heat of the star C_V , the total neutrino luminosity L_ν and the momentum of inertia I [3, 8]

$$P_G = \frac{32\pi (m-1)^{2m} (m+2)^{2m+2}}{((2m+1)!!)^2 (m+1)^{2m+2}} \tilde{J}_m^2 G M^2 R^{2m+2} \alpha^2 \Omega^{2m+4}, \quad (4)$$

$$P_S = -\frac{(m-1)(2m+1) \tilde{S}_m \Lambda_{\text{QCD}}^{3+\sigma} R^3 \alpha^2 \Omega^2}{T^\sigma}, \quad (5)$$

$$P_B = -\frac{16m}{(2m+3)(m+1)^5 \kappa^2} \frac{\tilde{V}_m \Lambda_{\text{QCD}}^{9-\delta} R^7 \alpha^2 \Omega^4 T^\delta}{\Lambda_{\text{EW}}^4}, \quad (6)$$

$$C_V = 4\pi \Lambda_{\text{QCD}}^{3-v} R^3 \tilde{C}_V T^v, \quad (7)$$

$$L_\nu = \frac{4\pi R^3 \Lambda_{\text{QCD}}^{9-\theta} \tilde{L}}{\Lambda_{\text{EW}}^4} T^\theta, \quad (8)$$

$$I = \tilde{I} M R^2. \quad (9)$$

where Λ_{QCD} and Λ_{EW} are characteristic strong and electroweak scales introduced to make these quantities dimensionless. With the energy of the r-mode

$$E_m = \frac{1}{2} \alpha^2 \Omega^2 M R^2 \tilde{J} \quad (10)$$

one can define characteristic time scales for the r-mode growth τ_G and the viscous damping τ_S and τ_B via

$$\frac{1}{\tau_i} = -\frac{P_i}{2E_m}. \quad (11)$$

so τ_G is negative and τ_S and τ_B are positive. The above quantities are given in terms of parameters that involve the integration over the star or alternatively over the layer ranging from R_i to R_o that contributes dominantly to this quantity. These are defined in table I.

All quantities appearing in these integrals, like the energy density ρ , the inverse squared speed of sound A , the non-equilibrium susceptibility C and the r-mode density oscillation

parameter of the ...	integral expression
moment of inertia	$\tilde{I} \equiv \frac{8\pi}{3MR^2} \int_0^R dr r^4 \rho$
radiated power	$\tilde{J}_m \equiv \frac{1}{MR^{2m}} \int_0^R dr r^{2m+2} \rho$
shear dissipated power	$\tilde{S}_m \equiv \frac{1}{R^{2m+1} \Lambda_{\text{QCD}}^{3+\sigma}} \int_{R_i}^{R_o} dr r^{2m} \tilde{\eta}$
bulk dissipated power	$\tilde{V}_m \equiv \frac{\Lambda_{\text{EW}}^4}{R^3 \Lambda_{\text{QCD}}^{9-\delta}} \int_{R_i}^{R_o} dr r^2 A^2 C^2 \tilde{\Gamma} (\delta \Sigma_m)^2$
specific heat	$\tilde{C}_V \equiv \frac{1}{R^3 \Lambda_{\text{QCD}}^{3-v}} \int_{R_i}^{R_o} dr r^2 \tilde{c}_V$
neutrino luminosity	$\tilde{L} \equiv \frac{\Lambda_{\text{EW}}^4}{R^3 \Lambda_{\text{QCD}}^{9-\theta}} \int_{R_i}^{R_o} dr r^2 \tilde{\epsilon}$

Table I: Radial integral parameters encoding the complete information on the star's interior - i.e. on the microphysical transport properties, the equation of state and the star's density profile.

$$\delta\Sigma \equiv \frac{m+1}{2\alpha R^2 \Omega^3} \sqrt{\frac{(m+1)^3 (2m+3)}{4m}} \left(\int d\Omega \left| \vec{\nabla} \cdot \delta\vec{v} \right|^2 \right)^{\frac{1}{2}} \quad (12)$$

depend on the position within the star via their density dependence. These few constants encode the complete information on the physics inside the star and are sufficient to calculate the star evolution.

The dimensionless parameters \tilde{I} and \tilde{J} , arising in the moment of inertia and the canonical energy and angular momentum of the mode, involve integrals over the energy density in which the outer parts are strongly weighted by high powers of r . They are normalized by the mass and appropriate powers of the radius so that the range these constants can vary over is independent of the mass. The mass by which these constants are divided is given by an analogous integral with a smaller power of r . Consequently these constants are large for stars whose mass is strongly spread out but small for stars where the mass is concentrated close to the center. Since the energy density is a monotonously decreasing function, it is clear that \tilde{I} and \tilde{J} are bounded from above by the values for a constant density star [3]. Similarly, lower bounds can be obtained by noting that in a star the mass cannot be arbitrarily concentrated. A limit for the energy density at a given radius is obtained by the constraint that the matter within this radius has to be stable against gravitational collapse. The corresponding bound for the energy density is given by $\rho(r) < 1/(8\pi G r^2)$ which can be integrated to obtain lower bounds on \tilde{I} and \tilde{J} . Combining these rigorous limits we find that for any compact star these parameters are narrowly bounded within roughly a factor of two

$$0.22 \approx \frac{2}{9} \leq \tilde{I} \leq \frac{2}{5} = 0.4, \quad (13)$$

$$1.59 \cdot 10^{-2} \approx \frac{1}{20\pi} \leq \tilde{J} \leq \frac{3}{28\pi} \approx 3.41 \cdot 10^{-2}. \quad (14)$$

However, for a neutron star with a crust the energy

density vanishes at the surface and therefore the upper bounds should even clearly overestimate the realistic range.

The uncertainty on the other parameters arises both from the microscopic quantities eqs. (2) and (3) as well as from the particular (baryon) density profile $n(r)$ which in turn depends both on the equation of state and the particular solution of the TOV equations (parameterized e.g. by the star's mass). All parameters defined above in tab. I are given for different stars in tab. II. For illustration of our semi-analytic results below we consider different stars with an APR equation of state [15]. In these stars we assume that the core of the star dominates the relevant quantities and neglect possible contributions from the crust. For the maximum mass APR star the density is high enough that direct Urca processes are kinematically allowed within an inner core.

III. PULSAR EVOLUTION

The evolution equations are obtained from energy and angular momentum conservation laws [8, 16] and take the form

$$\frac{d\alpha}{dt} = -\alpha \left(\frac{1}{\tau_G} + \frac{1}{\tau_V} \left(\frac{1 - Q\alpha^2}{1 + Q\alpha^2} \right) \right), \quad (15)$$

$$\frac{d\Omega}{dt} = -\frac{2\Omega Q\alpha^2}{\tau_V} \frac{1}{1 + Q\alpha^2}, \quad (16)$$

$$\frac{dT}{dt} = -\frac{1}{C_V} (L_\nu - P_V), \quad (17)$$

with $Q \equiv 3\tilde{J}/(2\tilde{I})$ and in terms of the viscous dissipated power $P_V = P_S + P_B + \dots$ and damping time $1/\tau_V \equiv 1/\tau_S + 1/\tau_B + \dots$, where the dots denote possible other dissipative mechanisms, like boundary layer effects. Here we include the reheating due to the dissipated power P_V within the star, that was partly neglected in [8]. Using the previous bounds on the parameters \tilde{I} and \tilde{J} we see that $Q < 81/(112\pi) \approx 0.23$ so that the factors $1 \pm Q\alpha^2$ are only relevant for large amplitude modes with $\alpha \gtrsim 1$, i.e. in a regime where the perturbative approximation for the r-mode [12] breaks down anyway. The r-mode is unstable when the right hand side of the amplitude equation eq. (15) is positive, i.e. when $\tau_V|_{\alpha=0} \geq -\tau_G$, where the equality defines the boundary of the instability region [3]. Since the r-mode will grow once it enters the instability region the evolution requires a non-linear mechanism to saturate the amplitude at a finite value. A simple possibility is the suprathermal enhancement of the bulk viscosity [4, 13, 17]. Unfortunately when only the damping in the core is considered, this mechanism saturates the mode only at rather large amplitudes. The bulk viscosity contribution of the inner crust might change this since the outer regions of the star are strongly weighted by the suprathermal viscosity [4], but the bulk viscosity has not been computed at this

neutron star	shell	$R [km]$	$\Omega_K [Hz]$	\tilde{I}	\tilde{J}	Q	\tilde{S}	\tilde{V}	\tilde{C}_V	\tilde{L}	σ	δ	v	θ
APR 1.4 M_\odot	core	11.5	6020	0.283	1.81×10^{-2}	0.096	7.68×10^{-5}	1.31×10^{-3}	2.36×10^{-2}	1.91×10^{-2}	$\frac{5}{3}$	6	1	8
APR 2.0 M_\odot		11.0	7670	0.300	2.05×10^{-2}	0.102	2.25×10^{-4}	1.16×10^{-3}	2.64×10^{-2}	1.69×10^{-2}				
APR 2.21 M_\odot	m.U. core	10.0	9310	0.295	2.02×10^{-2}	0.103	5.05×10^{-4}	9.34×10^{-4}	2.62×10^{-2}	1.29×10^{-2}	$\frac{5}{3}$	4	1	6
	d.U. core							1.16×10^{-8}		$2.31 \cdot 10^{-5}$				

Table II: Parameters characterizing the neutron star considered in this work. The constants \tilde{I} , \tilde{J} , \tilde{S} , \tilde{V} , \tilde{C}_V and \tilde{L} are given in tab. I using the generic normalization scales $\Lambda_{\text{QCD}} = 1 \text{ GeV}$ and $\Lambda_{\text{EW}} = 100 \text{ GeV}$ and the temperature exponents σ , δ , v and θ are defined by eqs. (2) and (3).

point. Another promising mechanism is the non-linear coupling of the r-mode to other daughter modes that are subsequently damped by viscosity [18]. Further possibilities include non-linear hydrodynamic effects [19, 20] or turbulent crust-core boundary layer damping [21] but at this point it is not settled which of these mechanisms will actually saturate the mode. Therefore, we follow here the approach pursued in [8] and will not study a particular saturation mechanism but simply assume that a corresponding mechanism operates and saturates the r-mode at a particular amplitude α_{sat} . In contrast to the above explicit mechanisms, α_{sat} is in this case an unknown parameter that may depend on Ω or T and we will study the dependence of our results on it below.

At saturation $d\alpha/dt = 0$ from eq. (15),

$$\frac{1}{\tau_V} = \frac{1}{\tau_G} \left(\frac{1 + Q\alpha^2}{1 - Q\alpha^2} \right) \xrightarrow{\alpha \ll 1/\sqrt{Q}} \frac{1}{\tau_G}, \quad (18)$$

and likewise $P_V \rightarrow P_G$. This simply says that at saturation there must be a sufficiently strong source of dissipation to overcome the gravitational instability. Making the replacements in eqs. (15), (16) and (17) leaves the reduced set

$$\frac{d\Omega}{dt} = -\frac{2\Omega}{|\tau_G|} \frac{Q\alpha_{\text{sat}}^2}{1 - Q\alpha_{\text{sat}}^2} \approx -\frac{2Q\alpha_{\text{sat}}^2\Omega}{|\tau_G|}, \quad (19)$$

$$\frac{dT}{dt} = -\frac{1}{C_V} \left(L_\nu + P_G \left(\frac{1 + Q\alpha_{\text{sat}}^2}{1 - Q\alpha_{\text{sat}}^2} \right) \right) \approx -\frac{1}{C_V} (L_\nu + P_G), \quad (20)$$

where, as argued before, the approximate expressions hold over nearly the entire range of physically reasonable amplitudes. Note that compared to [8] we take into account that the saturation mechanism dissipates according to eq. (18) a significant amount of energy that heats the star. The only way that this could be avoided is if some of the corresponding energy is radiated away, e.g. in neutrinos or electromagnetic radiation. In all proposed mechanisms, like the non-linear enhancement of the bulk viscosity [4, 17], mode-coupling to viscously damped daughter modes [18] or nonlinear hydrodynamic effects [19, 20], this is not the case and the dissipated energy eventually entirely ends up as heat.

The complete information on the saturation mechanism is then encoded in the saturation amplitude which

can be a general function $\alpha_{\text{sat}}(T, \Omega)$. This function has to vanish at the boundary of the instability region. Due to the strong power law dependence of the corresponding time scales τ_G and τ_V on T and Ω , it drops sharply over a very narrow region, as has been explicitly shown in [4]. For the spindown evolution this narrow boundary region is far less important than the much larger interior of the instability region. In the interior the amplitude will depend much more weakly on T and Ω and we make the simple power law ansatz

$$\alpha_{\text{sat}} = \hat{\alpha}_{\text{sat}} T^\beta \Omega^\gamma. \quad (21)$$

For instance the semi-analytic expression for the saturation amplitude due to suprathermal bulk viscosity has such a power law dependence on the frequency and proves to be even independent of temperature, i.e. $\beta = 0$ [4]. Since the only temperature dependence in eq. (19) comes from the implicit dependence via α_{sat} , for $\beta = 0$ the spindown evolution is not affected at all by the thermal evolution. This applies in particular to the model employed in [8] where the saturation amplitude is assumed to be constant throughout the instability region.

To analyze the above equations it is useful to introduce characteristic evolution time scales

$$\tau_\alpha \equiv -\alpha \left(\frac{d\alpha}{dt} \right)^{-1}, \quad \tau_\Omega \equiv -\Omega \left(\frac{d\Omega}{dt} \right)^{-1}, \quad \tau_T \equiv -T \left(\frac{dT}{dt} \right)^{-1}. \quad (22)$$

A young compact star is born in a core bounce supernova with a large temperature $T > 10^{11} \text{ K}$. We will assume that the initial frequency is above the minimum frequency of the instability region [3]. Initially $\tau_T \sim T^{-(\theta-v-1)}$ is small so that the star cools very fast due to neutrino emission and quickly enters the instability region. There by definition $|\tau_G| < \tau_V|_{\alpha=0}$ and (while the star cools further) the r-mode will grow with time scale $\tau_\alpha \approx \tau_G$. For a compact star spinning with a millisecond period this scale is of the order of seconds, so that the amplitude quickly grows until it is saturated at some α_{sat} . From this point on the fast evolution of α stops and it changes slowly with temperature and frequency. Since cooling is initially very quick but slows down considerably at lower temperatures, at some point the temperature-independent dissipation eq. (18) required to saturate the mode will dominate. The important question for the evolution is then if the spin-

down or the temperature change is faster. To see this let us analyze the behavior when temperature change due to dissipative heating (neglecting neutrino emission) $\tau_T^{(H)}$ is faster than the spindown, i.e. $\tau_T^{(H)} < \tau_\Omega$. This condition yields a relation for the angular velocity of the star which introducing the Kepler frequency $\Omega_K = \frac{4}{9}\sqrt{2\pi G\rho_0}$ can be written in the form

$$\frac{\Omega}{\Omega_K} > \frac{27}{8\pi} \sqrt{\frac{\tilde{C}_V}{\tilde{I}(1 - Q\alpha_{\text{sat}}^2)} \frac{R}{R_S} \frac{\Lambda_{\text{QCD}}^4}{\bar{\rho}}} \left(\frac{T}{\Lambda_{\text{QCD}}}\right)^{v+1} \xrightarrow{v=1} \text{const} \frac{T}{\Lambda_{\text{QCD}}}, \quad (23)$$

where in the second line we use the fact that for dense matter in general the temperature exponent arising in the specific heat eq. (3) obeys $v \geq 1$, and larger values make the right hand side even smaller. For a compact star the constant is $O(1)$, since the dimensionless parameters \tilde{C}_V and \tilde{I} are normalized to also be $O(1)$, the characteristic scale for the average energy density $\bar{\rho}$ of strongly interacting matter is Λ_{QCD}^4 , the radius of a neutron star is close to its Schwarzschild radius $R_S = 2GM$ and the root further decreases deviations from unity. However, since a compact star is a degenerate system, after a short time it reaches a temperature where $T/\Lambda_{\text{QCD}} \lesssim O(10^{-3})$. Therefore, taking into account the $O(1)$ prefactor, the viscous heating should be faster than the spindown for frequencies $\Omega/\Omega_K \gtrsim 10^{-2}$. Since r-modes are only present within the instability region, this should be compared to the minimum of the instability region Ω_{min} , for which a semi-analytic expression is given in [3]. There it was shown that this minimum is extremely insensitive to the microscopic details which yields a general limit of roughly $\Omega_{\text{min}}/\Omega_K \gtrsim 1/20$. Therefore, at r-mode saturation within the instability region the dissipative heating is always faster than the spindown. Note that this conclusion is generic and to leading order independent of both the saturation amplitude and the composition of the star.

IV. SEMI-ANALYTIC EXPRESSIONS

A. Endpoint of the evolution

Since for a compact star the thermal evolution is faster than the spindown, the evolution of the star should follow a curve $\Omega_{hc}(T)$ where it is always thermally in a steady state where neutrino cooling equals viscous heating $L_\nu + P_G = 0$ [18]. With the semi-analytic expressions eqs. (4) and (8) this equation can be solved explicitly and yields for the dominant $m = 2$ r-mode

$$\Omega_{hc}(T) = \left(\frac{3^8 5^2}{2^{15}} \frac{\tilde{L} \Lambda_{\text{QCD}}^{9-\theta} T^{\theta-2\beta}}{\tilde{J}^2 \Lambda_{\text{EW}}^4 G M^2 R^3 \hat{\alpha}_{\text{sat}}^2} \right)^{1/(8+2\gamma)}. \quad (24)$$

The evolution should therefore follow this curve until the star leaves the instability region. As can be seen in fig. 1, the boundary of the instability region of a neutron star has different segments: a low-temperature boundary outside of which shear viscosity damps the mode and an intermediate-temperature boundary where bulk viscosity is the dominant damping mechanism. Since the bulk viscosity features a resonant behavior and decreases again at very large temperatures $T \gtrsim 10^{11}$ K, there is a third high-temperature boundary above which the r-mode is unstable (see fig. 3 of [3]), but for neutron stars this segment is quite likely physically irrelevant since the stars cool below it quickly. Semi-analytic expressions for these segments of the boundary of the instability region have been derived in [3]. The form of the boundary depends strongly on the form of matter. When exotic forms of matter are present then in the relevant temperature regime there are so called stability windows, caused by the resonant behavior of the bulk viscosity of the corresponding phase, where the star is stable against developing an r-mode up to large frequencies (see fig. 3 of [3]). In case the steady-state curve formally lies in such a stability window it would clearly be irrelevant for the spindown¹. Then the evolution can take a long time, since the strong heating can push the star out of the instability region before the r-mode reaches a large amplitude, and other spindown sources will likely dominate. Therefore we will restrict ourselves here to the case of pure neutron stars. The general evolution for different forms of matter will be discussed elsewhere.

In the case of neutron stars the intermediate-temperature boundary of the instability region has a steeper slope than the steady state curve which thereby can only intersect the low-temperature boundary. In the case of a neutron star the low-temperature boundary $\Omega_{lb}(T)$ is determined by the condition $\tau_S = \tau_G$ and the corresponding semi-analytic solution is [3]

$$\Omega_{lb}(T) = \left(\frac{3^8 5^3}{2^{17} \pi} \frac{\tilde{S} \Lambda_{\text{QCD}}^{3+\sigma}}{\tilde{J}^2 G M^2 R^3 T^\sigma} \right)^{1/6}. \quad (25)$$

The final angular velocity Ω_f where the evolution leaves the instability region is given by

$$\Omega_f = \left(\left(\frac{3^8 5^3}{2^{17} \pi} \right)^{\theta+\sigma-2\beta} \left(\frac{4\pi}{5} \right)^\sigma \times \frac{\tilde{S}^{\theta-2\beta} \tilde{L}^\sigma \Lambda_{\text{QCD}}^{3\theta+9\sigma-6\beta-2\beta\sigma}}{\left(\tilde{J}^2 G M^2 R^3 \right)^{\theta+\sigma-2\beta} \Lambda_{\text{EW}}^4 \hat{\alpha}_{\text{sat}}^{2\sigma}} \right)^{1/(6\theta+8\sigma+2\gamma\sigma-12\beta)}, \quad (26)$$

¹ As just noted, for standard neutron stars the corresponding stability window lies at very large temperatures $T > 10^{10}$ K where the neutrino cooling still strongly dominates.

and the corresponding temperature T_f reads

$$T_f = \left(\left(\frac{3^8 5^3}{2^{17} \pi} \right)^{2+2\gamma} \left(\frac{5}{4\pi} \right)^6 \right. \\ \left. \times \frac{\tilde{S}^{8+2\gamma} \Lambda_{\text{EW}}^{24} \Lambda_{\text{QCD}}^{-30+6\theta+8\sigma+6\gamma+2\gamma\sigma} \hat{\alpha}_{\text{sat}}^{12}}{\tilde{L}^6 (\tilde{J}^2 G M^2 R^3)^{2(1+\gamma)}} \right)^{1/(6\theta+8\sigma+2\gamma\sigma-12\beta)}. \quad (27)$$

Note that, if we had used a different steady-state curve $\Omega_{hc}^{(S)}$ where the heating comes only from shear viscosity, as assumed in [8], or if we had included the bulk viscosity as well, the rest of the evolution could be very different, but we would have obtained exactly the same result for the endpoint eqs. (26) and (27) of the evolution. This surprising feature comes about since the shear viscosity is strongly dominant compared to the bulk viscosity on the left boundary and this boundary is precisely defined by the condition $\tau_S = \tau_G$ which implies that dissipated power equals the power radiated in gravitational waves $P_S = P_G$. In this sense the result eq. (26) is universal and does not depend on assumptions about the dissipative aspects of the saturation mechanism.

The above expressions involve the star constants given in tab. II. In order to give these expressions in a more physical form we write them relative to a fiducial reference model chosen as a $1.4 M_\odot$ neutron star with an APR equation of state [15] given in the first row of tab. II and denoted by a subscript “fid”. In case of a constant, T - and Ω -independent, saturation amplitude [8] $\beta = \gamma = 0$ this gives for a *standard* neutron star (*NS*) with shear viscosity due to leptonic processes and neutrino emission due to modified Urca reactions

$$T_f^{(NS)} \approx (1.26 \cdot 10^9 \text{ K}) \left(\frac{\tilde{S}}{\tilde{S}_{\text{fid}}} \right)^{3/23} \left(\frac{\tilde{L}}{\tilde{L}_{\text{fid}}} \right)^{-9/92} \left(\frac{\tilde{J}}{\tilde{J}_{\text{fid}}} \right)^{-3/46} \\ \times \left(\frac{M}{1.4 M_\odot} \right)^{-3/46} \left(\frac{R}{11.5 \text{ km}} \right)^{-9/92} \alpha_{\text{sat}}^{9/46}, \quad (28)$$

$$f_f^{(NS)} \approx (61.4 \text{ Hz}) \left(\frac{\tilde{S}}{\tilde{S}_{\text{fid}}} \right)^{3/23} \left(\frac{\tilde{L}}{\tilde{L}_{\text{fid}}} \right)^{5/184} \left(\frac{\tilde{J}}{\tilde{J}_{\text{fid}}} \right)^{-29/92} \\ \times \left(\frac{M}{1.4 M_\odot} \right)^{-29/92} \left(\frac{R}{11.5 \text{ km}} \right)^{-87/184} \alpha_{\text{sat}}^{-5/92}. \quad (29)$$

First it is interesting to note that all these expressions depend neither on the specific heat nor directly on the bulk viscosity of the considered form of matter. The latter is at first sight surprising since the bulk viscosity is the dominant dissipation mechanism at high temperatures and low amplitudes. But during the spindown evolution the dissipation is dominated by the appropriate saturation mechanism while the amount of dissipation is according to eqs. (11) and (18) determined entirely by gravitational physics. This is particularly favorable since it eliminates the complications arising from

the fact that the damping due to bulk viscosity requires the density fluctuation of the r-mode eq. (12) which is only non-vanishing to second order in Ω [12] and involves significant uncertainties. Even more striking is the extreme insensitivity of these result to the remaining microphysics included in the constants \tilde{S} and \tilde{L} . The neutrino emissivity constant \tilde{L} , in particular, depends on poorly known strong interaction corrections to the weak processes [22]. Yet, the remarkably small power $5/184$ arising in the important expression for the final angular velocity $\Omega_f^{(NS)}$ almost eliminates this uncertainty. The dependence of $\Omega_f^{(NS)}$ on the shear viscosity constant \tilde{S} is somewhat stronger but \tilde{S} is dominated by electromagnetic leptonic processes [23] that are well under theoretical control² and depends on the equation of state only via the lepton densities. The dependence on the parameters \tilde{J} , M and R which encode macroscopic properties of the star is stronger, but they vary only within narrow margins. This insensitivity to the underlying parameters is similar to the case of the minimum of the instability region analyzed previously in [3], yet it is fortunately even more pronounced in the physically important case eq. (29). The most striking feature of these expression, however, is that the insensitivity extends even to the dependence on α_{sat} , which is theoretically uncertain by many orders of magnitude [4, 18–20] and therefore represents the main uncertainty in the analysis. Here the similarly small power $5/92$ dramatically reduces this dependence and thereby allows a quantitative comparison with observational data below.

To get an idea of the uncertainty in $f_f^{(NS)}$ we estimate the error ranges of the individual parameters by symmetric logarithmic error bands - i.e. we allow for the corresponding parameter to be smaller or larger than the APR reference star by a given factor. The shear viscosity parameter \tilde{S} due to leptonic processes [23] is uncertain within a factor of two of \tilde{S}_{fid} and the neutrino emissivity parameter \tilde{L} due to modified Urca processes [22] within an order of magnitude of \tilde{L}_{fid} . For \tilde{J} we have rigorous limits eq. (14). An upper limit for the mass of a neutron star is $\lesssim 2.5 M_\odot$ and an upper limit for the radius of a star rotating with millisecond periods about $\lesssim 15 \text{ km}$. Since the upper bound for \tilde{J} is for a constant density profile which is far from the situation in a neutron star and, due to cancellations, the dependence on the mass and radius turns out to be significantly weaker than these individual individual errors suggest, see table III below, we consider half the above ranges for the individual logarithmic uncertainties for \tilde{J} , M and R as a more realistic estimate. Under the assumption that these errors are independent we find

² There is a hadronic contribution to the shear viscosity as well but the latter is strongly subleading at temperatures relevant to young neutron stars due to the different power law dependence.

$$f_f^{(NS)} \approx (61.4 \pm 9.4) \text{ Hz } \alpha_{\text{sat}}^{-5/92}. \quad (30)$$

We want to stress that this is just an estimate of the likely error range and not a statistical measure of well defined significance.

Different classes of compact stars, containing other phases of dense matter with different low energy degrees of freedom, feature different values for the exponents in eqs. (2) and (3) and can lead to qualitatively different behavior. An example is a heavy star where direct Urca reactions are kinematically allowed in an inner core and the parameters change according to table II which increases the final frequency beyond the above error range. When exotic forms of matter are present, like hyperon or quark matter, the enhanced dissipation of these phases leads to stability windows [3, 24]. In this case the boundary of the stability window in the relevant temperature regime is determined by the bulk viscosity of the exotic phase, so that eqs. (26) and (27) are not valid. The steady state curve then ends at a higher frequency due to the instability window where the star leaves the unstable regime and cools until it reaches the lower boundary of the stability window. Since at these lower temperatures r-mode heating dominates neutrino cooling the star is repeatedly pushed out of the instability region once its amplitude becomes large and the residual spindown takes much longer [25, 26]. The important point is however, that the final frequency which is in this case given by the minimum of the instability region and for which a similarly precise semi-analytic result exists [3] is systematically larger for exotic forms of matter since the strong bulk viscosity of the exotic phase dominates the shear viscosity down to lower temperatures. Therefore, the above expressions eqs. (29) and (30) provide lower bounds for the frequency to which an arbitrary compact star can be spun down due to the r-mode instability.

B. Evolution time scales

Next let us actually solve the evolution equations to obtain the corresponding evolution time scales. The initial cooling time in the stable regime before the evolution enters the instability region t_{sc} results from solving the thermal equation eq. (17), in the absence of damping, down to the temperature determined by the semi-analytic expression for the intermediate-temperature boundary of the instability region given in [3]. The result reads

$$t_{sc} = \frac{1}{\theta - v - 1} \left(\frac{3^3 5^2}{2^{12} 7 \pi \kappa^2} \right)^{(\theta - v - 1)/\delta} \times \left(\frac{\tilde{V}_m^{\theta - v - 1} \tilde{C} \Lambda_{\text{QCD}}^{9(\theta - v - 1) - 5\delta} R^{\theta - v - 1}}{\tilde{L}^\delta \Lambda_{\text{EW}}^{4(\theta - \delta - v - 1)} (\tilde{J}^2 G M^2 \Omega_i^4)} \right)^{1/\delta} \quad (31)$$

in terms of the initial angular velocity Ω_i and depends both on the bulk viscosity and the specific heat. For a standard neutron star with shear viscosity due to leptonic processes and neutrino emission due to modified Urca reactions this gives

$$t_{sc}^{(NS)} \approx (7.83 \cdot 10^{-2} \text{ s}) \left(\frac{\tilde{V}}{\tilde{V}_{\text{fid}}} \right) \left(\frac{\tilde{J}}{\tilde{J}_{\text{fid}}} \right)^{-2} \left(\frac{\tilde{C}}{\tilde{C}_{\text{fid}}} \right) \left(\frac{\tilde{L}}{\tilde{L}_{\text{fid}}} \right)^{-1} \times \left(\frac{M}{1.4 M_\odot} \right)^{-2} \left(\frac{R}{11.5 \text{ km}} \right) \left(\frac{f_i}{\text{kHz}} \right)^{-4}. \quad (32)$$

This time is so short compared to the subsequent r-mode evolution that it can safely be neglected.

The spindown time t_{sd} is obtained by solving the frequency equation eq. (19) in the saturated regime. As noted before, this equation completely decouples for $\beta = 0$ and factoring the frequency dependence out of the gravitational time scale via $\tau_G \equiv \tilde{\tau}_G \Omega^{-6}$ yields the frequency solution

$$\Omega(t) = \left(\Omega_i^{-6-2\gamma} - \frac{4(3+\gamma) Q \tilde{\alpha}_{\text{sat}}^2 t}{\tilde{\tau}_G} \right)^{-1/(6+2\gamma)}. \quad (33)$$

We find in terms of the gravitational time scale eq. (4) evaluated at the minimum frequency

$$t_{sd} = - \frac{\tau_G(\Omega_f)}{12(1+\gamma/3) Q \alpha_{\text{sat}}^2(\Omega_f)} \left(1 - \left(\frac{\Omega_f}{\Omega_i} \right)^{6+2\gamma} \right) \xrightarrow{\Omega_f \ll \Omega_i} - \frac{1}{6(1+\gamma/3)} \frac{\Omega_f}{\tilde{\Omega}_f}. \quad (34)$$

If the saturation amplitude has a frequency dependence with exponent $\gamma < 0$, then up to small corrections in Ω_f/Ω_i this simply increases the spindown time compared to a constant saturation amplitude by a factor³ $1/(1+\gamma/3)$. In case of dissipation due to suprathermal bulk viscosity [4] the spindown time is longer compared to the saturation model with a constant amplitude by a factor of 9/5.

The above expression eq. (34) looks similar to the relation between the spindown time for other spindown mechanisms, like magnetic dipole radiation or gravitational wave emission due to deformations, and the characteristic pulsar time scale $-\Omega_0/\dot{\Omega}_0$ [5]. Yet, the important point to note here is, that Ω_f and $\dot{\Omega}_f$ are the values before the star leaves the instability region which can be very different from the observed values Ω_0 and $\dot{\Omega}_0$ if the observation is performed after the star has left the instability region. The characteristic feature of the r-mode

³ In the case $\gamma = -3$ the spindown equation eq. (19) would give a logarithmic instead of a power law solution, yet this special case does not seem physically relevant.

mechanism, namely that it operates only for a finite time interval, renders the r-mode spindown time completely independent of the characteristic pulsar time scale and allows the former to be orders of magnitude smaller, since the spindown rate can strongly drop from a large r-mode rate to a much lower rate of other spindown mechanisms at the boundary of the instability region.

Inserting the expression for the final frequency eq. (34) into eq. (29) this yields in case of a standard neutron star and for $\Omega_f \ll \Omega_i$

$$t_{sd}^{(NS)} \approx (12.3 \text{ y}) \left(\frac{\tilde{S}}{\tilde{S}_{\text{fid}}} \right)^{-18/23} \left(\frac{\tilde{L}}{\tilde{L}_{\text{fid}}} \right)^{-15/92} \left(\frac{\tilde{J}}{\tilde{J}_{\text{fid}}} \right)^{-5/46} \\ \times \left(\frac{\tilde{I}}{\tilde{I}_{\text{fid}}} \right) \left(\frac{M}{1.4 M_{\odot}} \right)^{41/46} \left(\frac{R}{11.5 \text{ km}} \right)^{-107/92} \alpha_{\text{sat}}^{-77/46}. \quad (35)$$

Here the dependence on the parameters is stronger so that the duration is considerably more uncertain. In particular it is very sensitive to the saturation amplitude α_{sat} . If α_{sat} becomes too small this time scale is so long that other spindown mechanisms will dominate, as is clear from the sizable observed spindown rate of young pulsars [27]. Employing the bounds eqs. (13) and (14) as well as the full uncertainty ranges for the other underlying parameters discussed before to estimate the uncertainty in the final frequency eq. (30) we find that the spindown time could be smaller or larger by nearly an order of magnitude.

V. SPINDOWN OF YOUNG PULSARS

A. Comparison of analytic and numeric results

The results for the evolution of the $1.4 M_{\odot}$ neutron star in temperature-angular velocity space is shown in fig. 1 for different values of the initial rotation angular velocity and the saturation amplitude. As can be seen the numerical solution given by the solid curves perfectly confirms the above picture. The star initially cools until it reaches the instability region, where the r-mode amplitude starts to grow. Once the amplitude is significant the star starts spinning down but since the spindown time τ_{Ω} is much longer than the cooling time τ_T , the star cools further until it reaches the steady state curve⁴ where the fast temperature evolution is stopped and the star evolves along the steady state curve on the longer time scale τ_{Ω} . Consequently, the evolution is completely

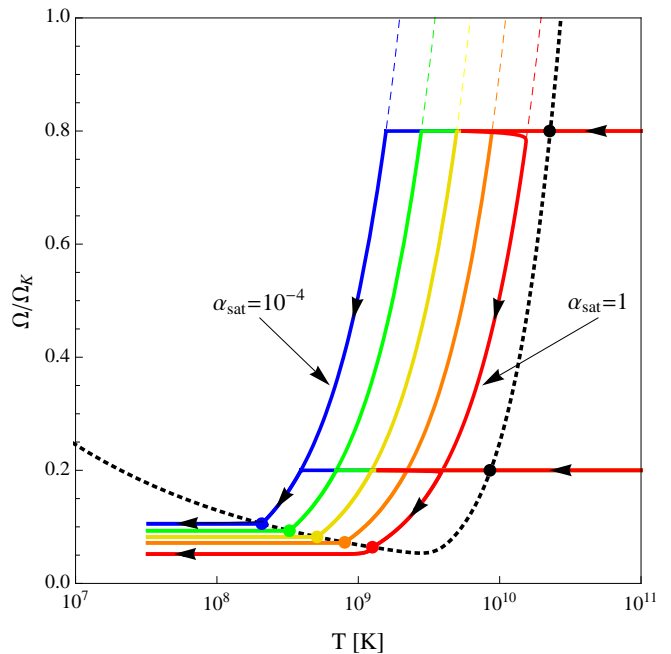


Figure 1: The spindown evolution of a young $1.4 M_{\odot}$ neutron star with an APR equation of state [15] in temperature-angular velocity space. The boundary of the instability region of the fundamental $m = 2$ r-mode is shown by the dotted curve. The dashed curves (which are mostly hidden underneath the solid curves) represent the steady state eq. (24) where heating equals cooling and are given for different r-mode amplitudes ranging from $\alpha_{\text{sat}} = 10^{-4}$ (left) to $\alpha_{\text{sat}} = 1$ (right). The solid lines show the numerical solution of the evolution equations for two fiducial initial spin frequencies $\Omega = 0.8 \Omega_K$ and $\Omega = 0.2 \Omega_K$. As can be seen, after an initial cooling phase the evolution simply merges on the appropriate steady state curve and follows it to the edge of the instability region. The dots denote the semi-analytic results for the points of the spindown evolution where the star enters and leaves the instability region, eqs. (28) and (29).

independent of the initial amplitude α_{min} required to start the growth in eq. (15). Such initial perturbations will clearly be present immediately after the creation of the neutron star following a core bounce. As anticipated, the numerical solution also proves that the evolution is to very good accuracy independent of the initial frequency unless it is very close to the final frequency. Therefore, similar to the thermal evolution, the spindown evolution completely loses its memory of the initial conditions at sufficiently late times. The saturation amplitude in contrast provides the dominant uncertainty for the evolution and the trajectory is shown for a range of possible saturation amplitudes. Larger values lead to stronger dissipative reheating and therefore spin down the star at larger temperatures so that the evolution leaves the instability region at lower frequencies closer to the minimum of the instability region. The dots are obtained from the analytic expressions eqs. (28) and (29) which agree with the numerical solution. Note again that we

⁴ For the largest saturation amplitudes the evolution reaches the steady state temperature before its amplitude has saturated. Therefore, as can be seen from the $\alpha_{\text{sat}} = 1$ curve in fig. 1, the star “undercools” to lower temperatures and then reheats back to the steady state curve once the saturation amplitude is reached.

neglect other spindown mechanisms like magnetic dipole radiation in this work which would speed up the evolution and continue the magnetic spindown after the star leaves the r-mode instability region.

In [8] the evolution was artificially stopped at a temperature of 10^9 K since superfluidity and non-perfect fluid effects were expected to invalidate the analysis below. We do not follow this ad hoc prescription here since it is not likely that these effects have such a big influence on the spindown evolution for the following reasons: One important effect of superfluidity is to affect beta equilibration. Around the critical temperature it is enhanced due to pair breaking, but at temperatures far below and small oscillation amplitudes beta equilibration processes are strongly suppressed. Since the superfluid gap depends strongly on density the entire star will not be gapped at such temperatures and therefore in part of the star the weak interactions are hardly affected and the corresponding parameters \tilde{L} and \tilde{V} are only moderately reduced. Even more, as has recently been shown in [14], superfluidity does not suppress weak processes at all at sufficiently large amplitudes that are within the range we study here. Superfluidity can also lead to an additional source of dissipation via mutual friction. In contrast to the earlier generic analysis referred to in [8], the later dedicated r-mode analysis [28] showed that it is unlikely that mutual friction has such a dramatic impact on the r-mode instability. In [29] this effect was studied, taking into account the large uncertainties in pairing and the microscopic drag parameter. It was found that depending on these uncertainties the effect can range from the unlikely extreme that the r-mode is completely suppressed below a certain temperature to a nearly negligible impact on the instability region compared to the ungapped case. Therefore, it is interesting to study the present case of standard dissipation sources in detail, since it sets the limit on the frequency to which r-modes can spin down a star as well as on the emitted gravitational wave signal, as discussed below. Any additional dissipation source will reduce the r-mode instability and correspondingly lead to larger final spin frequencies and a smaller gravitational wave signal.

Fig. 2 shows the evolution of the angular velocity as a function of time. As predicted by eq. (35), the spindown time increases strongly with decreasing saturation amplitude. The points show that the semi-analytic results for this time again agree with the numerical solution⁵. Here we are mainly interested in the spindown

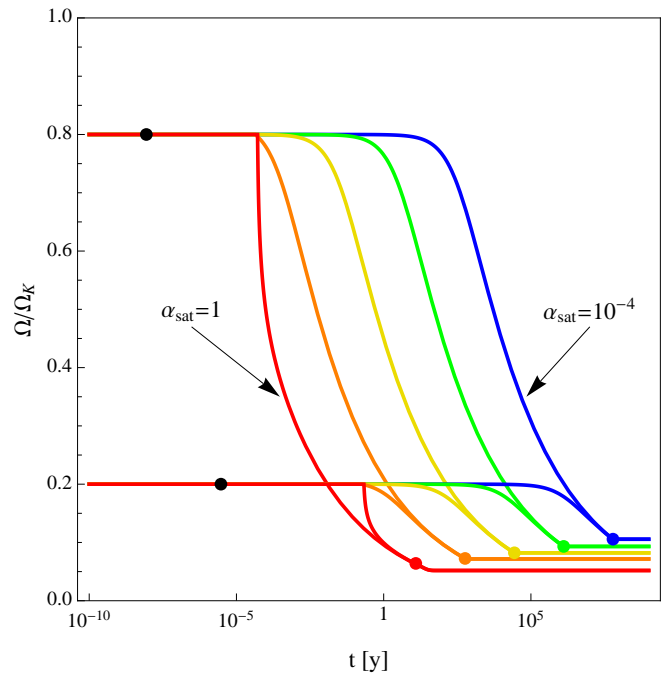


Figure 2: The spindown evolution of a young neutron star. The solid lines show the evolution of a $1.4 M_\odot$ star with an APR equation of state and for different amplitudes ranging from $\alpha_{\text{sat}} = 1$ (left) to $\alpha_{\text{sat}} = 10^{-4}$ (right). The dots denote the analytic results eq. (32) respectively eqs. (35) and (29) for the point of the spindown evolution where the star enters and leaves the instability region.

aspects and only note that as far as the thermal evolution is concerned the r-mode effectively causes a delay in the cooling. This is significant initially, but, since the cooling slows down strongly, it is irrelevant at later times $t \gg t_{sd}$.

Table III lists the semi-analytic results for a range of saturation amplitudes for two different neutron stars - the previously discussed standard star with a canonical mass of $1.4 M_\odot$ and, motivated by the recent observation [30], also a heavy $2.0 M_\odot$ star. Strikingly the final frequency proves nearly independent of the mass, and is far less sensitive than eq. (29) naively suggests. This is apparently caused by cancellations due to the implicit mass dependence of the radius and of the parameters \tilde{J} , \tilde{S} and \tilde{L} . Despite the explicit normalizations in table I these parameters still have a significant implicit dependence on M and R via the density profile of the star. Correspondingly, whereas the dependence on microscopic material properties is explicitly given by the semi-analytic expressions eqs. (26) to (35), the dependence on star properties like the mass and radius is not properly reflected by the explicit dependencies alone but the additional implicit

⁵ Note that the spindown overshoots at large amplitude since it takes time for the amplitude to decay and the spindown continues during this period, as can be seen from the lowest curve which drops below the dot so that the final frequency lies somewhat below the instability region. This is mainly an artifact of the simplified model which keeps the amplitude constant until the instability boundary is reached. In reality with an explicit saturation mechanism the amplitude has to vanish at the boundary in

the static limit, so it must start decreasing inside the instability region, see [4].

α_{sat}	T_f [10^8 K]	Ω_f/Ω_K	f_f [Hz]	t_{sd} [y]
1	12.6 (13.9)	0.064 (0.049)	61.4 (60.3)	12.3 (9.4)
0.1	8.02 (8.88)	0.073 (0.056)	69.5 (68.4)	582 (445)
10^{-2}	5.11 (5.66)	0.082 (0.063)	78.8 (77.5)	$2.75 (2.10) \cdot 10^4$
10^{-3}	3.26 (3.61)	0.093 (0.072)	89.3 (87.8)	$1.30 (0.99) \cdot 10^6$
10^{-4}	2.08 (2.30)	0.106 (0.081)	101.2 (99.5)	$6.11 (4.68) \cdot 10^7$

Table III: Dependence of the results obtained from the semi-analytic expressions for the characteristic quantities eqs. (28), (29) and (35) of the spindown evolution for neutron star with an APR equation of state on the saturation amplitude α_{sat} . We give in each case results for both a standard $1.4 M_\odot$ star and a heavy $2.0 M_\odot$ star next to it in parentheses. At the smallest amplitudes the given spindown times t_{sd} should not be relevant since they would be so long that the neglected magnetic spindown should dominate and spin down the star on much shorter time scales.

dependence via the averaged quantities in table I is crucial. The initial cooling time before the star enters the instability region is amplitude independent and yields for a star spinning at the Kepler frequency the small values $t_{sc} = 96.4$ (55.1) ms, which rise to a few hours for frequencies at the lower end of the instability region, which is indeed negligible compared to the long spindown times. The left part of table IV finally compares the spindown observables for different stars at a fixed amplitude $\alpha_{sat} = 1$. We see that, when direct Urca processes are allowed, the final temperature is significantly lower due to the enhanced neutrino cooling. Since the instability region shrinks at lower temperatures the final frequency is higher and the spindown time is correspondingly shorter.

B. Saturation model dependence

Let us now discuss the influence of different saturation models $\alpha_{sat}(T, \Omega)$. Since in the general case eq. (21) the amplitude varies over the instability region and the coefficient $\hat{\alpha}_{sat}$ is a dimensionful parameter, we have to find analogous parameter values for $\hat{\alpha}_{sat}$ to compare saturation models with different values of β and γ among each other and with the constant model discussed so far. Since the evolution spends most of the time in the final stages of the spindown evolution it is natural to choose $\hat{\alpha}_{sat}$ so that different models have a similar amplitude in this stage. If we compare models defined by $\hat{\alpha}_{sat}$, β and γ that have the same amplitude α_{sat} at the end of the evolution, then they leave the instability region at the same point given by eqs. (26) and (27). This can be easily seen, noting that the conditions $\tau_S = \tau_G$ and $P_S = P_G$ that determine the endpoint depend only on the saturation amplitude $\alpha_{sat}(T_f, \Omega_f)$ at this point. However, the path within the instability region, determined by the steady state curve eq. (24), and in particular the thermal behavior will depend on β and γ .

Fig. 3 shows a few examples of different saturation

models for two different saturation amplitudes $\alpha_{sat} = 10^{-4}$ and $\alpha_{sat} = 1$ at the end of the evolution. The solid lines are the constant model $\beta = \gamma = 0$ [8] discussed above. The dashed curves show the case when suprathermal viscosity is strong enough to saturate the mode. In this case the analytic result for the amplitude is $\alpha_{sat} \sim \Omega^{-4/3}$ [4] and the amplitude becomes large at low frequency where the suprathermal enhancement of the viscosity is weaker. Since the amplitude is lower at large frequency the dissipative heating is smaller and the steady state curve moves to lower temperatures. Since the spindown evolution is in this case still independent of temperature, the spindown time eq. (35) does not change compared to the constant model and the only difference is in the thermal evolution within the instability region. The thermal evolution could further be altered by the suprathermal enhancement of the neutrino emissivity [14] that we neglect here.

The final example is a case where the amplitude rises with temperature $\alpha_{sat} \sim T$. This seems to be realized to some extent in mode-coupling models, where the saturation amplitude is as low as $\alpha_{sat} = O(10^{-5})$ in the low temperature regime relevant for low mass X-ray binaries [31] which is smaller than in the high temperature regime relevant for young stars where $\alpha_{sat} = O(10^{-3} - 10^{-2})$ [18]. As shown by the dot-dashed curves ($\beta = 1$, $\gamma = 0$) in fig. 3, the steady-state curve lies at higher temperatures⁶. Because of the temperature dependence of the saturation amplitude in eq. (19) this could now actually change the spindown time. However, there is only a significant increase of the amplitude at high temperatures and thereby higher frequencies. Since the evolution is fast in this region anyway this would hardly affect the overall spindown time. Therefore, we do not expect a qualitative change of the picture presented above in this case either⁷.

In conclusion, different saturation mechanisms could change the thermal evolution but should not change the spindown behavior within the uncertainty range for the saturation amplitude from the picture obtained above with a constant amplitude. Furthermore, eq. (26) shows that the observed insensitivity to the microscopic parameters is not strongly altered by the saturation model for

⁶ In mode coupling models the saturation amplitude also has a frequency dependence with a negative exponent which would counteract the temperature effect and bring the curve closer to the constant model again.

⁷ At large saturation amplitudes the steady state curve crosses the instability boundary at an angular velocity below the Kepler frequency (see the rightmost curve in fig. 3). This could in principle result in a qualitatively different initial evolution that oscillates around the boundary since strong reheating is pushing the evolution out of the instability region. Yet in this case the amplitude at high temperatures is unphysically large. Note that the amplitude is limited by energy constraints to values $\lesssim O(1)$ since the mode energy cannot become bigger than the rotational energy.

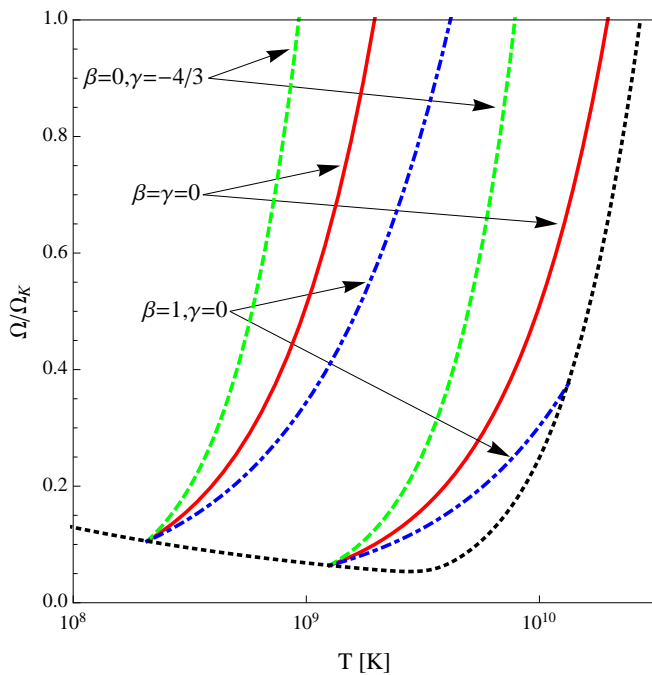


Figure 3: The dependence of the steady-state curve eq. (24) on the saturation model for two different saturation amplitudes $\alpha_{\text{sat}}(T_f, \Omega_f) = 10^{-4}$ (left curves) and 1 (right curves) at the end of the evolution. The solid line shows the model with constant amplitude $\beta = \gamma = 0$ [8], the dashed line denotes the case $\beta = 0, \gamma = -4/3$ corresponding to saturation by non-linear bulk viscosity [4] and the dotted curve shows a fiducial model with $\beta = 1, \gamma = 0$ which might capture certain features of the saturation model via mode coupling [18, 31].

realistic values $|\beta|, |\gamma| \ll \theta$.

C. Comparison to pulsar data

The semi-analytic expressions finally allow us to compare our theoretical results to observational data. In most analyses [32, 33], merely the observed pulsar frequencies are compared to numerical computations of the r-mode instability region. For stars which spin slow enough that they are clearly below the minimum of the instability region this shows that they cannot have r-mode oscillations at present. However, there is at least one young star which lies above the minimum of the instability region. Since the instability boundary is strongly temperature dependent, information on the temperature of fast stars is required to decide if they are actually inside the instability region. Yet, the temperature is unknown for most pulsars. Therefore, we will here go beyond such a static analysis and take into account the dynamic evolution as well as the frequency eq. (26) where the star actually leaves the instability region.

In addition to the spin frequencies also the spindown rates are known for many young stars. Naturally, this additional information provides a stronger constraint on

spindown models. The time derivative of the frequency is readily obtained from eq. (19). Fig. 4 compares the spindown evolution for different saturation amplitudes to the data for young stars that still have a significant spindown rate. As can be seen there is one pulsar J0537-6910 that spins fast enough that it could be within the instability region of a standard neutron star whose minimum frequency is denoted by the vertical dotted line to the left⁸. Taking into account the dynamical evolution, the additional knowledge of the spindown rate alleviates the uncertainty with respect to the saturation amplitude, since larger amplitudes lead to significantly larger spindown rates. This is shown by the black line which is formed by the semi-analytic results for the endpoints of the evolution and which represents the boundary of the instability region in f - \dot{f} -space. The gray band reflects the uncertainty in the underlying parameters eq. (30). The fastest pulsar J0537-6910 is obviously compatible with being outside of the instability region. Thereby no observed star lies definitely inside the instability region which confirms the r-mode scenario for a sufficiently short spindown time. Moreover, J0537-6910 lies clearly below the line for our APR neutron star and just at the lower edge of the uncertainty band. Therefore, very likely no young star observed so far currently emits gravitational waves because of the r-mode instability. This is strengthened by the absence of gravitational wave signals from observed young pulsars - including in particular J0537-6910 - in the latest LIGO data [34].

Our analysis was performed for a standard neutron star, but the instability regions for other possible exotic forms of matter do not extend to such low frequencies and thereby cannot change the conclusion that the observed stars are out of the instability region. Due to the insensitivity of the final frequency eq. (26) to the underlying parameters this should be a robust result and could be explicitly confirmed once a braking index for J0537-6910 can be measured. As a consequence our result shows that the r-mode picture of the spindown of young pulsars presents a viable explanation for the low spin rates of young pulsars if the saturation amplitude is large enough $\alpha_{\text{sat}} > 0.01$ to spin down the pulsar in a time $t_{\text{sd}} < 10^4$ y. An upper limit for the saturation amplitude $\alpha_{\text{sat}} < 1$ comes from the observed timing data of J0537-6910, as noted in [35], since r-modes would have otherwise spun it down to its current frequency in less than a hundred years which is much shorter than its age estimate [36]. Whereas the r-mode picture yields a quantitative explanation for the maximum observed spin frequency, other mechanisms, like the possibility that all stars are already born with lower frequencies or the subsequent spindown via magnetic dipole radiation, have as

⁸ The analytic result for the minimum of the instability region given in [3] would allow us to estimate also the uncertainties on the minimum frequency, but we refrain from this for better readability.

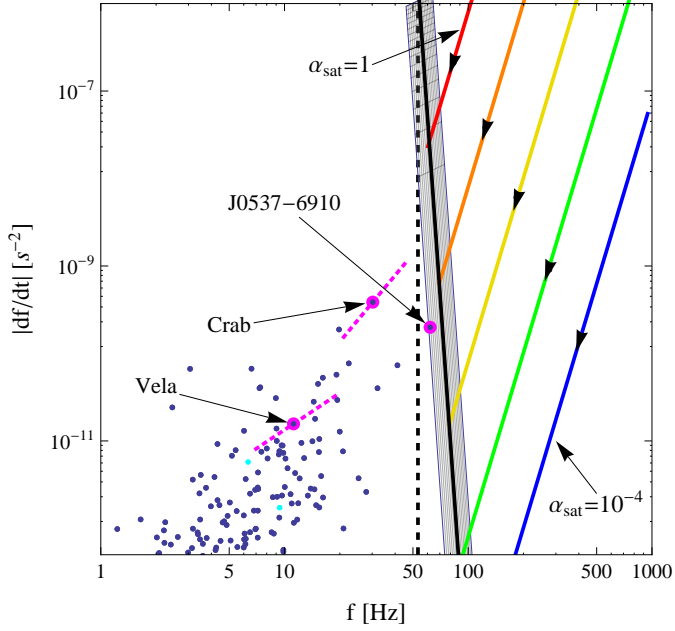


Figure 4: The spindown evolution of a young neutron star compared to observed pulsar data from the ATNF catalog [27]. The solid lines show the evolution of the $1.4 M_{\odot}$ star for different saturation amplitudes ranging from $\alpha_{\text{sat}} = 1$ (top) to $\alpha_{\text{sat}} = 10^{-4}$ (bottom). The vertical dashed line to the left shows the lower frequency boundary of the instability region. The steep solid line is formed by the endpoints of the evolution for different values of α and thereby represents the boundary of the instability region in f - \dot{f} -space, whereas the gray band reflects the error due to the uncertainty in the underlying parameters. The dotted line segments show the current evolution for two stars for which a reliable braking index is available [5, 37].

far as we know not provided a robust explanation why fast stars with a small initial magnetic dipole moment resulting in a slow spindown could not form.

VI. GRAVITATIONAL WAVE EMISSION

As discussed in the previous section, all presently observed young pulsars are likely outside of the instability region and so should not emit gravitational radiation due to r-modes. Nevertheless, it is possible that in the future we may observe a young pulsar that is still in the unstable region. Furthermore, gravitational waves might even be detected from so far unknown young compact stars that have not been seen because their electromagnetic radiation is either too faint or it is absorbed or outshined by the supernova remnant. This possibility is interesting since there are several known young supernova remnants, including most notably SN 1987A, where a compact object has not been observed, yet. In view of the upcoming next generation of gravitational wave detectors like advanced LIGO [9] it is therefore important to understand

the expected gravitational radiation of such sources in detail.

Above we already gave semi-analytic expressions for two important quantities in this respect, namely the rotational angular velocity Ω_f eq. (26) when the star exits the r-mode instability region, which is related to the lower bound ν_f of the gravitational wave spectrum via $\nu = 2/(3\pi)\Omega$, and the spindown time t_{sd} eq. (34), which is the maximum age up to which gravitational waves from such a source could be observed. For a standard neutron star eq. (30) we estimate $\nu_f \approx (81.9 \pm 12.5) \text{ Hz } \alpha_{\text{sat}}^{-5/92}$. To have a reliable estimate for the lower bound of the spectrum is particularly important since advanced LIGO will have a significantly improved sensitivity below 100 Hz which coincides with the final stages of the r-mode spindown. Since the r-mode evolution becomes slow at low frequencies this region is where the evolution spends the most time and the analytic expression for the spindown time as a function of the dependent parameters should then allow us to estimate the probability that sources within the reach of advanced LIGO are currently active and observable.

A. Gravitational emission due to r-modes

In this section we follow the previous analysis [8] and provide a similar semi-analytic expression for the gravitational wave strain emitted in the final stage of the spindown. An analytic result for the gravitational wave strain, averaged over polarizations and the orientation and position of a source at distance D on the sky, was given in [8, 38]

$$h(t) = \sqrt{\frac{3}{80\pi}} \frac{\omega^2 S_{22}}{D} \quad (36)$$

with the mass current quadrupole moment

$$S_{22} = \sqrt{2} \frac{32\pi}{15} G M \alpha \Omega R^3 \tilde{J} \quad (37)$$

However, those authors did not determine the cutoff frequency analytically. Using our result eq. (26) we find for the final gravitational wave strain emitted in the last stage of the evolution

$$h_f = \sqrt{\frac{2^{15}\pi}{3^5 5^3}} \frac{\tilde{J} G M R^3 \alpha_{\text{sat}} \Omega_f^3}{D} \quad (38)$$

in terms of the final frequency Ω_f eq. (26). For a neutron star the final gravitational strain is

$$h_f^{(NS)} \approx 7.23 \cdot 10^{-27} \alpha_{\text{sat}}^{\frac{77}{92}} \left(\frac{\text{Mpc}}{D} \right) \quad (39)$$

The emitted gravitational wave strain during the evolution is shown in fig. 5 for different values of the saturation

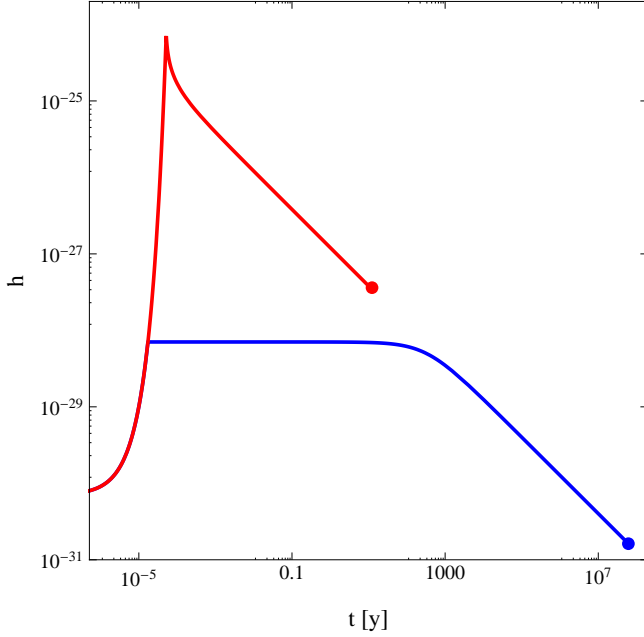


Figure 5: The gravitational wave strain of a $1.4 M_{\odot}$ APR neutron star located somewhere in the Virgo cluster (distance 20 Mpc). Shown are the numerical curves for two different r-mode saturation amplitudes $\alpha_{\text{sat}} = 1$ (top) and $\alpha_{\text{sat}} = 10^{-4}$ (bottom). The dots denote the analytic result eq. (38) for the minimum strain amplitude of the gravitational radiation emitted at the end of the r-mode evolution and the endpoints for other amplitudes lie on the line through these two points.

amplitude. The numerical curves are compared to the analytic results for the minimum gravitational strain at the end of the evolution eq. (39) denoted by the points. As can be seen small amplitude r-modes have a lower maximum amplitude but emit low amplitude gravitational waves over longer times.

For an actual detection a systematic search strategy is required which takes into account the periodic structure of the signal. In ref. [8] matched filtering was considered as a possible method. Since it requires prior knowledge of the detailed form and time evolution of the signal which might not be feasible, the estimates for the signal-to-noise ratio using this method are an optimistic estimate for more realistic methods. To compare the gravitational strain to current detector bounds the Fourier-transformed gravitational wave strain $\tilde{h}(\nu)$ in the frequency domain is the relevant quantity. It can be obtained in a stationary phase approximation as

$$\left| \tilde{h}(\nu) \right|^2 = \left| h(t) \right|^2 \left| \frac{dt}{d\nu} \right| \quad (40)$$

As seen from fig. 5, there are two qualitatively different stages of the gravitational wave emission. The first arises from the growth phase of the r-mode and results in narrow spike in $\tilde{h}(\nu)$ at the stars initial frequency. This

phase lasts only for a short time of order minutes and as shown in [8] there is not enough energy in this pulse to be detectable. Therefore, we neglect this initial part of the spectrum here. In the subsequent saturated phase where the star spins down it emits gravitational waves over a continuous frequency range with corresponding strain

$$\tilde{h}(\nu) = \sqrt{\frac{9\tilde{I}GMR^2}{20D^2\nu}} \quad (41)$$

The quantity that can directly be compared to the detector sensitivity, described by the rms strain noise $h_{\text{rms}} \equiv \sqrt{\nu S_h(\nu)}$ in terms of the power spectral density⁹ S_h of the detector noise, is the characteristic amplitude of the signal defined by $h_c \equiv \nu \tilde{h}$. In particular the minimum characteristic amplitude $h_{c,f} \equiv h_c(\nu_f)$ reached at the lower frequency boundary of the evolution reads in the saturated regime

$$h_{c,f} = \sqrt{\frac{3\tilde{I}GMR^2}{10\pi D^2}} \left(\left(\frac{3^8 5^3}{2^{17} \pi} \right)^{\theta+\sigma-2\beta} \left(\frac{4\pi}{5} \right)^{\sigma} \right. \quad (42) \\ \left. \times \frac{\tilde{S}^{\theta-2\beta} \tilde{L}^{\sigma} \Lambda_{\text{QCD}}^{3\theta+9\sigma-6\beta-2\beta\sigma}}{\Lambda_{\text{EW}}^{4\sigma} (\tilde{J}^2 GM^2 R^3)^{\theta+\sigma-2\beta} \hat{\alpha}_{\text{sat}}^{2\sigma}} \right)^{1/(4(3\theta+4\sigma+\gamma\sigma-6\beta))}$$

The square root in eq. (41) makes the dependence of $h_{c,f}$ on the microscopic parameters even weaker than for the final frequency eq. (29). However, the expression depends more strongly on macroscopic quantities like the mass and the moment of inertia encoded in the parameter \tilde{I} . The rigorous bounds eq. (13) show that this dependence is also moderate since all these quantities vary only within roughly a factor of two. For a standard neutron star we find

$$h_{c,f}^{(NS)} \approx 1.6 \cdot 10^{-22} \left(\frac{\tilde{S}}{\tilde{S}_{\text{fid}}} \right)^{3/46} \left(\frac{\tilde{L}}{\tilde{L}_{\text{fid}}} \right)^{5/368} \left(\frac{\tilde{J}}{\tilde{J}_{\text{fid}}} \right)^{-29/184} \\ \times \left(\frac{\tilde{I}}{\tilde{I}_{\text{fid}}} \right)^{1/2} \left(\frac{M}{1.4 M_{\odot}} \right)^{63/184} \left(\frac{R}{11.5 \text{ km}} \right)^{281/368} \left(\frac{\text{Mpc}}{D} \right) \alpha_{\text{sat}}^{-5/184}$$

Note that this quantity is nearly independent of the saturation amplitude α_{sat} (and even increases with decreasing amplitude). The same holds for the microscopic parameters. For example the dependence on the neutrino emissivity involves the power 5/368 which provides a striking example of how insensitive such macroscopic observables can be to microscopically decisive yet inherently poorly

⁹ The “power spectral density” is just the square of the amplitude spectral density of the noise expressed in equivalent gravitational wave strain, as given e.g. by the LIGO collaboration [39].

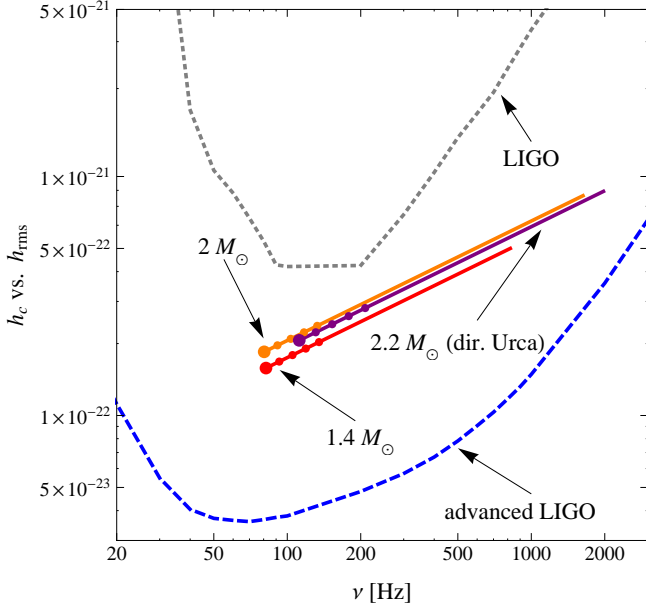


Figure 6: The characteristic gravitational wave amplitude of neutron stars, located somewhere in the Virgo cluster (distance 20 Mpc) and based on the different APR stars given in tab. II, compared to the sensitivity of the LIGO (dotted) and advanced LIGO (dashed) [9] detectors. The large dots denote the analytic expressions for the lower frequency limit for an amplitude $\alpha_{\text{sat}} = 1$ and the smaller ones for lower amplitudes down to $\alpha_{\text{sat}} = 10^{-4}$.

known quantities, since even a drastic change by three orders of magnitude would only have an irrelevant effect of less than 10%. In order for the characteristic amplitude to give a meaningful estimate the observation time should be comparable to the time scale of the frequency change of the signal (so that all strength of a given frequency is actually detected). Clearly for small saturation amplitudes where the spindown time increases drastically with decreasing α_{sat} , see eq. (35) and table III, this is not guaranteed and therefore the fact that the characteristic amplitude is above the background alone is not sufficient for a detection.

The result for the characteristic amplitude in the saturated regime is given for different stars in fig. 6. Whereas the spectra of the two standard neutron stars with modified Urca reactions have nearly the same lower frequency cutoff, the heavy star with direct Urca interactions in the core has a higher cutoff > 100 Hz, but otherwise features a characteristic amplitude of similar size, as could have been expected from the insensitivity to the neutrino emissivity in eq. (42).

B. Theoretical signal detectability

The signal to noise ratio for matched filtering can be written as [8]

$$\left(\frac{S}{N}\right)^2 \Big|^{(\text{tot.})} = 2 \int_{\nu_{\min}}^{\nu_{\max}} \frac{d\nu}{\nu} \left(\frac{h_c}{h_{\text{rms}}}\right)^2 = \frac{9I}{10D^2} \int_{\nu_{\min}}^{\nu_{\max}} \frac{d\nu}{\nu S_h(\nu)} \quad (43)$$

in terms of the power spectral density S_h of the noise and ranging over a range from the final frequency of the r-mode evolution $\nu_{\min} = \nu_f$ to the initial frequency $\nu_{\max} = \nu_i$ at which the star is created. Here the label (tot.) has been added to indicate that the total frequency spectrum is included in this quantity. This point will be discussed in more detail below. In eq. (43) logarithmic frequency intervals are weighted by $1/S_h$, since at low frequencies the frequency changes slowly which makes it easier to detect the periodic signal. Based on early estimates of the noise strain of a next generation LIGO detector and the assumption that r-modes are absent below 10^9 K, resulting in a large $\nu_{\min} \approx 120$ Hz, the initial analysis [8] approximated the background noise by simple power law $S_h \sim \nu^2$. Consequently, they found that the integral is completely dominated by the low frequency end and the dominant quantity is the minimum frequency - which would surely be most welcome in view of the analytic expression eq. (29). They find for the anticipated second generation LIGO detector [8]

$$\frac{S}{N} \Big|_{\text{Owen et. al.}}^{(\text{tot.})} \approx 8.8 \left(\frac{I}{10^{45} \text{cgs}}\right)^{1/2} \left(\frac{D}{20 \text{Mpc}}\right)^{-1} \left(\frac{\nu_{\min}}{120 \text{Hz}}\right)^{-1} \quad (44)$$

Yet, the anticipated design spectrum of the advanced LIGO background [9] improved compared to these early estimates. The noise has a minimum at $\nu \approx 300$ Hz and increases again towards lower frequencies. Therefore, even for a large lower cutoff frequency assumed in [8] the above integral is now dominated by intermediate frequencies which requires a more careful evaluation. After a numerical integration an approximate fit to the result over the relevant parameter ranges for ν_{\min} and ν_{\max} is given by¹⁰

$$\frac{S}{N} \Big|_{\text{aLIGO}}^{(\text{tot.})} \approx 4.09 \cdot 10^{23} \sqrt{\text{Hz}} \frac{\sqrt{GI}}{D} \times \sqrt{1 + 0.40 \log\left(\frac{\nu_{\max}}{1000 \text{Hz}}\right) + 0.36 \frac{100 \text{Hz} - \nu_{\min}}{100 \text{Hz}}} \quad (45)$$

i.e. we find a much weaker dependence on the minimum final frequency and a stronger dependence on the un-

¹⁰ We fit the integrated form rather than the initial strain noise S_h , since this provides a more precise result. Fitting the strain noise with a double power law $S_h(\nu) \approx a\nu^{-2} + b\nu^2 + c$, similar to the ansatz used in [35] before their subsequent approximation, we can perform the integration analytically, yielding the same qualitative leading parameter dependence on ν_{\min} (power law) and ν_{\max} (logarithmic) we use for the fit in eq. (45).

known maximum initial frequency. By inserting the result for the minimum frequency eq. (29) we see that the uncertainty of this result due to the microphysics is minor. The main uncertainty arises from the moment of inertia which using the above bounds has a maximum theoretical uncertainty of a factor of 4 but the actual range should again be smaller.

The signal to noise ratios for different sources at different distances are shown in table IV. Here we compare the values for sources given by the different considered stars, namely the $1.4 M_\odot$ and $2 M_\odot$ APR stars for which only modified Urca reactions are possible and the $2.2 M_\odot$ star where direct Urca reactions are present within its core. These are assumed to be located at different distances, namely in the Virgo Cluster (20 Mpc), the Local group of galaxies (1 Mpc) and within the Milky way (30 kpc). Using the actual anticipated noise background of the advanced LIGO detector and without the assumption that the evolution stops at 10^9 K, our values are slightly larger than those obtained in [8]. Heavier stars tend to give larger values due to the larger moment of inertia whereas direct Urca processes reduce the signal to noise ratio since the thermal steady-state curve is at lower temperatures and its intersection with the boundary of the instability region is correspondingly at a higher frequency that sets the lower gravitational wave frequency cutoff in eq. (45). Yet, overall these values are rather similar for the different considered stars. These considerations suggest that theoretically a detection is possible for sources up to large distances in case the gravitational wave signal could be detected over its complete frequency range.

C. Practical signal detectability

Although the above signal to noise ratios might give some measure for the relation of the total signal that is observable from such sources and the detector background, they do not directly reflect the detectability of the signal of a given single source over the actual observation period, as noted already in [8]. They would provide such an actual measure for the detectability only for a short multi-wavelength signal that is completely observed, for example a binary inspiral. Yet, they cannot give a reasonable measure in the present case where the source is monochromatic and changes slowly with time while it is only observed for a short time interval, since the frequency ranges in eq. (43) that would only be detectable hundreds of years before or after the present observation can hardly affect the detectability within the limited observation interval. Therefore a proper signal to noise ratio that measures the detectability must take into account the finite duration of the observation and only include the relevant frequencies in eq. (43).

To find such a reliable signal to noise ratio for the detectability in gravitational wave detectors, assume that the frequency of the source changes only slightly during the short observation time interval Δt over which it has

an average frequency $\bar{\nu}$. The change $\Delta\nu \ll \bar{\nu}$ during this time interval can be obtained from eq. (19)

$$\Delta\nu \approx \frac{2}{3\pi} \frac{d\Omega}{dt} \Delta t = \frac{2\bar{\nu}Q\alpha_{\text{sat}}^2}{\tau_G(\bar{\Omega})} \Delta t \quad (46)$$

The current angular velocity $\bar{\Omega}$ can be obtained in terms of the current age t of the star from the solution of the spindown equation eq. (19) which yields in the limit $\Omega_i \gg \bar{\Omega}$

$$\Delta\nu \approx -\frac{\bar{\nu}}{6} \frac{\Delta t}{t} \quad (47)$$

For $\Delta\nu \ll \bar{\nu}$ the integral in eq. (43) gives an estimate for the actual *observable* signal to noise ratio

$$\left. \frac{S}{N} \right|^{(\text{obs.})} \approx \sqrt{\frac{9\tilde{I}GMR^2}{10D^2} \frac{\Delta\nu}{\bar{\nu}S_h(\bar{\nu})}} = \sqrt{\frac{3GI}{20S_h(\bar{\nu})D^2} \frac{\Delta t}{t}} \quad (48)$$

This quantity depends on the observation time interval Δt (see also [40]) and depends on the internal composition of the star only via the moment of inertia with the resulting uncertainty for the signal to noise ratio of a factor of 4 noted above. Moreover, it depends only on the present (averaged) gravitational wave frequency $\bar{\nu}$ and not the complete spectrum. Strikingly it is again not directly dependent on the saturation amplitude which only enters indirectly via the dependence on the current frequency via $S_h(\bar{\nu})$. Yet, we stress again that this expression is only valid during the later evolution where the spindown becomes sufficiently slow so that $\Delta\nu \ll \bar{\nu}$. The right part of table IV shows the values for the advanced LIGO detector for the different stars and a ratio $\Delta t/t = 10^{-3}$ compared to the previous signal-to-noise estimates. As can be seen in this case the observable signal to noise ratios are more than two orders of magnitude smaller than the total expressions eq. (45).

For the advanced LIGO detector the background is nearly constant over the relevant range from 80 to 800 Hz with $S_h^{1/2} \approx 4 \cdot 10^{-24}$ and thereby allows us to further approximate to obtain the simple estimate

$$\left. \frac{S}{N} \right|_{\text{aLIGO}}^{(\text{obs.})} \approx 2.5 \sqrt{\frac{\Delta t}{t}} \left(\frac{20 \text{ Mpc}}{D} \right) \quad (49)$$

I.e. for a one year observation period, comparable to past LIGO runs, a source in the Virgo cluster (20 Mpc) would be impossible to detect unless it is very young. A source in our local group of galaxies (1 Mpc) in contrast might be detectable if the results obtained assuming matched filtering do not strongly overestimate the detectability for more realistic search methods. A source in the Milky Way (30 kpc) in contrast should be detectable even if a

neutron star	T_f [K]	f_f [Hz]	ν_f [Hz]	t_{sd} [y]	h_f @ 1 Mpc	$h_{c,f}$ @ 1 Mpc	$\frac{S}{N} _{\text{Virgo}}^{(tot)}$	$\frac{S}{N} _{\text{L.g.}}^{(tot)}$	$\frac{S}{N} _{\text{M.w.}}^{(tot)}$	$\frac{S}{N} _{\text{Virgo}}^{(obs)}$	$\frac{S}{N} _{\text{L.g.}}^{(obs)}$	$\frac{S}{N} _{\text{M.w.}}^{(obs)}$
APR 1.4 M_\odot	$1.26 \cdot 10^9$	61.4	81.8	12.3	$7.2 \cdot 10^{-27}$	$1.6 \cdot 10^{-22}$	11.7	234	7794	0.084	1.7	56
APR 2.0 M_\odot	$1.39 \cdot 10^9$	60.3	80.4	4.9	$9.7 \cdot 10^{-27}$	$1.8 \cdot 10^{-22}$	14.0	281	9356	0.099	2.0	66
APR 2.21 M_\odot	$3.15 \cdot 10^8$	84.0	112	1.7	$2.2 \cdot 10^{-26}$	$2.1 \cdot 10^{-22}$	12.7	254	8460	0.094	1.9	62

Table IV: Results for the spindown and gravitational wave observables for different neutron stars considered in this work obtained from the semi-analytic expressions eqs. (27), (26), (34), (38), (42) and (43). In contrast to the lower mass stars, the 2.21 M_\odot neutron star is dense enough to allow for direct Urca reactions. All values are given for a large saturation amplitude $\alpha_{sat} = 1$. The signal to noise ratios are given for the advanced LIGO detector and are obtained with the gravitational wave frequency corresponding to the Kepler frequency as an upper cutoff of the spectrum respectively a fiducial observation interval $\Delta t/t = 10^{-3}$. They are given for sources at three different distances ranging from the Virgo cluster (20 Mpc), and the local group of galaxies (1 Mpc) to a source within the Milky Way (30 kpc).

more realistic search strategy has a significantly lower signal to noise ratio. Since the original LIGO detector had a more than an order of magnitude larger background it is less surprising than for the previous estimate eq. (44) that no signal has been detected so far. As shown in the previous section the r-mode spindown scenario requires a sufficiently large amplitude leading to a sufficiently short spindown time so that after a long observation time of several years, the sensitivity could still be sufficient to detect pulsars that are currently in the r-mode phase. Future third generation gravitational wave detectors like the currently planned Einstein telescope [41] are expected to exceed advanced LIGO in sensitivity by an order of magnitude and thereby should allow us to see many more potential sources. This should mark the advent of gravitational wave astronomy and could allow us to learn about the composition of compact objects by gravitational wave observations. In this endeavor the simple semi-analytic expressions given here might prove useful.

Finally let us estimate likely values for the above signal to noise ratio for a few examples of known possible sources that could be young enough to emit gravitational waves due to r-modes. These consist of, in addition to the fastest pulsar J0537-6910 discussed above, the young neutron star Cassiopeia A from which no pulsation has been observed and several supernova remnants where no compact object has been detected so far. However, it has recently been suggested that the hard x-ray emission from SN 1957D results from a pulsar wind nebula and the compact remnant which produced it would then be the youngest indirectly observed pulsar [42]. The bounds for the moment of inertia again introduce an uncertainty of at most a factor of 4. As can be seen despite the fact that the observable signal-to-noise ratio eq. (49) is reduced by more than an order of magnitude compared to the total versions eqs. (44) and (45) the values are still large since all of these object are rather near. Even though the original LIGO had an order of magnitude weaker sensitivity the values are with the exception of SN 1957D and J0537-6910 large enough that it should have seen gravitational wave emission from these objects. Therefore it is very likely that these objects are not compact stars that spin fast enough to be in the unstable region. The proba-

bly youngest pulsar, produced by SN 1957D, would be an ideal candidate, but it is most likely too distant to clearly detect gravitational waves due to r-mode emission with advanced LIGO in its standard configuration. However, the further improved sensitivity of advanced LIGO in a narrowband mode [9] could increase the signal-to-noise ratio above the detection level. Therefore, focussing on the frequency range in table V, this source might present a promising candidate for such an in-depth search, provided that the observation interval is long enough that the sensitivity gain is not outweighed by the limited data. In case the fastest directly observed young pulsar J0537-6910 is still in the final stage of its r-mode evolution there is a good chance that its signal was just below the threshold of the original LIGO detector and will be detected by advanced LIGO.

VII. CONCLUSIONS

We have derived general semi-analytic results for the key quantities of the spindown evolution of young pulsars that reveal the dependence of these observables on the relevant physical ingredients. We find that the final spin frequency eq. (26) and the minimum gravitational wave strain emitted at the end of the evolution eq. (38) are remarkably insensitive to the microphysical material properties. For other input quantities like the moment of inertia of the star or the angular momentum of the mode we gave rigorous bounds that allow us to estimate the uncertainty in these parameters. We show that the thermal evolution is always faster than the spindown evolution. Therefore, if the form of the instability region is convex a steady state is reached where viscous heating equals cooling due to neutrino emission. Non-convexity of the instability region due to stability windows arising from enhanced dissipation due to exotic phases of matter can prevent the star from reaching the thermal steady state and thereby drastically change the evolution which could lead to clear astrophysical signatures.

The semi-analytic results for the final frequency of the evolution enabled a quantitative comparison to pulsar timing data and we find that all stars except one lie clearly below the frequency to which r-modes can spin

source	age [y]	D [kpc]	$\bar{\nu}$	h	h_c	$\frac{S}{N} _{\text{LIGO}}^{(obs)}$	$\frac{S}{N} _{\text{aLIGO}}^{(obs)}$	$\frac{S}{N} _{\text{aLIGO}}^{(tot)}$
J0537-6910	?	52	83	$1.4 (0.1) \times 10^{-26}$	$6.5 (6.8) \times 10^{-20}$	2.1 (0.2)	28 (2.8)	—
SN 1987A	25	51.5	157 (337)	$9.9 (1.0) \times 10^{-26}$	$0.8 (1.2) \times 10^{-19}$	23 (18)	221 (236)	$2.0 (3.2) \times 10^3$
SN 1957D	55	4610	137 (296)	$0.7 (2.3) \times 10^{-28}$	$0.9 (1.3) \times 10^{-21}$	0.2 (0.1)	1.6 (1.8)	19 (33)
G1.9+0.3	≈ 140	7.7	117 (157)	$2.8 (0.3) \times 10^{-25}$	$4.9 (7.2) \times 10^{-19}$	57 (62)	598 (662)	$0.9 (1.8) \times 10^4$
Cassiopeia A	≈ 300	3.4	104 (223)	$4.3 (0.4) \times 10^{-25}$	$1.0 (1.5) \times 10^{-18}$	83 (106)	906 (1015)	$1.3 (3.7) \times 10^4$
SN 1604	≈ 400	6.1	99 (213)	$2.1 (0.2) \times 10^{-25}$	$5.7 (8.3) \times 10^{-19}$	39 (53)	433 (488)	$0.6 (2.0) \times 10^4$
SN 1572	≈ 440	2.8	97 (209)	$4.3 (0.4) \times 10^{-25}$	$1.2 (1.8) \times 10^{-18}$	80 (111)	894 (1013)	$1.0 (4.3) \times 10^4$

Table V: Expected gravitational wave signal for different young sources in case there is an associated fast rotating compact object that spins down via the r-mode mechanism. All values are given for the $1.4 M_{\odot}$ APR star model with $\alpha_{\text{sat}} = 0.1$ (0.01) - for $\alpha_{\text{sat}} = 1$ r-modes would have had already decayed at the current age of these systems. The observable signal-to-noise ratios are computed assuming an observation time $\Delta t = 1$ y. The frequencies $\bar{\nu}$ are obtained from eq. (33) in the limit that the unknown initial frequency was much larger than the current one. The theoretical total signal-to-noise ratios are here obtained by taking into account the total frequency interval $[\nu_f, \bar{\nu}]$ that is observable from the stars current age to the end of the r-mode spindown.

down a young pulsar. Only the fastest spinning young star PSR J0537-6910 is fast enough that it could lie within the instability region. Using additional observation of spindown rates we find that this is unlikely since it lies just at the lower border of the uncertainty range. The spindown time in contrast depends strongly on the saturation amplitude and increases quickly from time scales of order years at $\alpha_{\text{sat}} \approx 1$ to more than a million years below $\alpha_{\text{sat}} < 10^{-3}$.

The r-mode scenario can therefore provide a quantitative explanation of the low spin frequencies of young pulsars if the saturation amplitude is within certain limits. On the one hand it has to be sufficiently large $\alpha_{\text{sat}} \gtrsim 0.01$ for the spindown to be fast enough to dominate other possible spindown mechanisms and result in spindown times that are shorter than the ages of observed pulsars of more than several hundred years. On the other hand, even taking into account the significant uncertainties, a very large saturation amplitude $\alpha_{\text{sat}} \approx 1$ would have spun PSR J0537-6910 down to its current frequency in less than a hundred years. This would be in clear conflict with the much larger age estimate of its remnant of roughly 5000 years [36] and the significant present spindown rate of the pulsar, which is most likely due to the electromagnetic radiation and should have further sped up the spindown. Different saturation scenarios do not significantly change the spindown time and therefore should not qualitatively affect our bounds on the saturation amplitude. In case r-modes reach sizable amplitudes $\alpha_{\text{sat}} \lesssim 0.1$, PSR J0537-6910 could be younger than its characteristic age - obtained within a pure magnetic dipole model - suggests. If in contrast r-modes saturate already at amplitudes $\alpha_{\text{sat}} < 0.01$ they would be subleading compared to the other spindown mechanisms, which must be sizable according to the significant spindown rates of observed young pulsars.

Since we find that likely no observed pulsar is at present spinning down due to r-modes, one has to be careful when interpreting spindown limits on r-mode amplitudes from young stars [35]. Although these limits give

important information on these stars, they are trivially fulfilled if the r-mode has already decayed. In this case the current rate involves only information on other spindown sources, like magnetic dipole emission, and cannot give a bound on the r-mode saturation amplitude during the era when r-modes were actually present. The spindown limit [35] simply extrapolates the solid lines in fig. 4 outside the instability region. In reality for a large saturation amplitude the star would actually spin down quickly inside but then the spindown rate would drop to a lower value determined by the other sources once the star leaves the instability region. The slope of the curves for other spindown mechanisms are generally smaller, as illustrated in fig. 4 for the Crab and the Vela pulsar where a reliable braking index is available, and can therefore be perfectly consistent with observations even for a large saturation amplitude during the r-mode phase as long as the star is currently already sufficiently far away from the instability boundary. Yet, in case of J0537-6910 which is still close to the instability boundary, the spindown limit is more restrictive and coincides with the limits above [35].

We considered in this work only the dominant $m = 2$ r-mode. The inclusion of higher multipoles might slightly affect the spindown time by a factor $\lesssim 1$ but will not change the final frequency since the corresponding instability regions of these modes are smaller [3] and therefore the final segment of the steady-state curve, where the evolution spends by far the longest time, is identical. Furthermore, we have here mainly studied the simplest case of a neutron star with minimal damping due to leptonic interactions and modified Urca processes in the core. The main reason for this is that it is the case of minimal damping whereas other phases of matter or structural inhomogeneities will increase the damping. Therefore, the final spindown frequencies we find are the lower limit to which general compact stars can be spun down by r-modes. In reality several aspects like pairing, mutual friction, the crust and other spindown mechanisms complicate the analysis. Although we did not study these

in detail here, our general semi-analytic expressions allow us to study any single source of damping, like the effect of an Ekman layer.

Nuclear pairing could strongly change the temperature dependence of material properties over the considered temperature regime so that it would not have a simple power law form. Therefore it should alter thermal evolution, but since at saturation the thermal evolution does - aside from the fact that its final frequency at the boundary of the instability region depends on temperature - not affect the spindown, the results presented here should not be strongly affected by pairing. The relevant part of the boundary is determined by shear viscosity which is dominated by electromagnetic leptonic processes which are only indirectly affected by the presence of hadronic matter. As found in [23] this is a moderate effect and taking into account the insensitivity of our results to the shear viscosity this should only slightly increase the considered error range.

As discussed before mutual friction in superfluid systems is an additional source of damping that could considerably shrink the instability region. If this effect is very strong it could significantly raise the frequency to which r-modes can spin down a star. As can be seen from fig. 1 if the enhanced damping is only present at low temperatures, e.g. $T < 10^9$ K as assumed in [8], this would strongly affect the evolution at low saturation amplitudes but only moderately at sufficiently large amplitudes favored above.

Furthermore, it has been argued that the boundary layer at the interface between the core and the crust strongly enhances the viscous damping which would reduce the r-mode instability region [43]. This mechanism is based on the picture that there is a sharp boundary and the fluid velocity drops to zero over a distance of a few centimeters. However, in reality the crust is a complicated structure with possible geometrically structured pasta phases and an inner crust where the concentration of the neutron fluid decreases continuously. The transition from a pure fluid to a rigid lattice then happens gradually over a large distance and it is questionable why the above picture should apply here. Phenomenologically these effects have partly been modeled via a slippage parameter and the impact becomes rather small for likely

parameter values [33]. We note, however, that our general analytic expressions should also apply when the crust provides the dominant source of dissipation. In this case further complications like the breaking or melting of the crust could be relevant which in turn should reduce the effect of viscous boundary layer damping.

Finally, we computed the gravitational wave emission due to the r-mode spindown of young stars. We updated the expressions previously given in [8] by employing the current advanced LIGO design background and find that this further decreases the dependence on the final frequency of the spindown analysis and thereby on the microphysics. Beyond this, we point out that a realistic signal-to-noise ratio should take into account that the signal is only observed for a limited time. The corresponding novel expression for the signal-to-noise ratio eq. (48) is proportional to the root of the ratio of the observation time and the age of the star and thereby becomes small for short observation times or old stars. For typical values we find that the signal-to-noise ratio is roughly two orders of magnitude smaller than the previous result. Although advanced LIGO would still be able to detect known nearby sources if they emit gravitational waves at present, this reduction limits the distance to which we can see such objects and thereby the number of observable sources. Nevertheless, both the steadily growing list of known young pulsars and the strongly increased sensitivity of next generation gravitational wave detectors like advanced LIGO could still make it possible to detect gravitational radiation due to r-modes, which would provide a unique way to learn about the internal composition of compact stars.

Acknowledgments

We are grateful to Brynmor Haskell, Prashant Jaikumar, Feryal Özel and Simin Mahmoodifar for helpful discussions. This research was supported in part by the Offices of Nuclear Physics and High Energy Physics of the U.S. Department of Energy under contracts #DE-FG02-91ER40628, #DE-FG02-05ER41375.

-
- [1] N. Andersson, *Astrophys. J.* **502**, 708 (1998), gr-qc/9706075.
 - [2] N. Andersson and K. D. Kokkotas, *Int. J. Mod. Phys. D* **10**, 381 (2001), gr-qc/0010102.
 - [3] M. Alford, S. Mahmoodifar, and K. Schwenzer, *Phys.Rev.* **D85**, 024007 (2012), 1012.4883.
 - [4] M. G. Alford, S. Mahmoodifar, and K. Schwenzer, *Phys.Rev.* **D85**, 044051 (2012), 1103.3521.
 - [5] S. L. Shapiro and S. A. Teukolsky, *Black holes, white dwarfs, and neutron stars: The physics of compact objects* (, 1983).
 - [6] J. Staff, P. Jaikumar, and R. Ouyed, *Astrophys.J.* **751**, 24 (2012), 1107.1000.
 - [7] F. E. Marshall, E. V. Gotthelf, W. Zhang, J. Middleditch, and Q. D. Wang, *Astrophys. J. Lett.* **499**, L179 (1998), arXiv:astro-ph/9803214.
 - [8] B. J. Owen *et al.*, *Phys. Rev.* **D58**, 084020 (1998), gr-qc/9804044.
 - [9] LIGO Scientific Collaboration, G. M. Harry, *Class.Quant.Grav.* **27**, 084006 (2010).
 - [10] N. Andersson *et al.*, *Gen.Rel.Grav.* **43**, 409 (2011), 0912.0384.

- [11] R. C. Tolman, Phys. Rev. **55**, 364 (1939).
- [12] L. Lindblom, G. Mendell, and B. J. Owen, Phys. Rev. **D60**, 064006 (1999), gr-qc/9902052.
- [13] M. G. Alford, S. Mahmoodifar, and K. Schwenzer, J. Phys. **G37**, 125202 (2010), 1005.3769.
- [14] M. G. Alford, S. Reddy, and K. Schwenzer, Phys.Rev.Lett. **108**, 111102 (2012), 1110.6213.
- [15] A. Akmal, V. R. Pandharipande, and D. G. Ravenhall, Phys. Rev. **C58**, 1804 (1998), nucl-th/9804027.
- [16] W. C. Ho and D. Lai, Astrophys.J. **543**, 386 (2000), astro-ph/9912296.
- [17] A. Reisenegger and A. A. Bonacic, (2003), astro-ph/0303454.
- [18] R. Bondarescu, S. A. Teukolsky, and I. Wasserman, Phys. Rev. **D79**, 104003 (2009), 0809.3448.
- [19] L. Lindblom, J. E. Tohline, and M. Vallisneri, Phys. Rev. Lett. **86**, 1152 (2001), astro-ph/0010653.
- [20] W. Kastaun, Phys.Rev. **D84**, 124036 (2011), 1109.4839.
- [21] Y. Wu, C. D. Matzner, and P. Arras, Astrophys.J. **549**, 1011 (2001), astro-ph/0006123.
- [22] B. L. Friman and O. V. Maxwell, Astrophys. J. **232**, 541 (1979).
- [23] P. S. Shternin and D. G. Yakovlev, Phys. Rev. **D78**, 063006 (2008), 0808.2018.
- [24] P. Jaikumar, G. Rupak, and A. W. Steiner, Phys. Rev. **D78**, 123007 (2008), 0806.1005.
- [25] J. Madsen, Phys. Rev. Lett. **85**, 10 (2000), astro-ph/9912418.
- [26] N. Andersson, D. I. Jones, and K. D. Kokkotas, Mon. Not. Roy. Astron. Soc. **337**, 1224 (2002), astro-ph/0111582.
- [27] R. N. Manchester, G. B. Hobbs, A. Teoh, and M. Hobbs, Astron. J. **129**, 1993 (2005), astro-ph/0412641.
- [28] L. Lindblom and G. Mendell, Phys.Rev. **D61**, 104003 (2000), gr-qc/9909084.
- [29] B. Haskell, N. Andersson, and A. Passamonti, (2009), 0902.1149.
- [30] P. Demorest, T. Pennucci, S. Ransom, M. Roberts, and J. Hessels, Nature **467**, 1081 (2010), 1010.5788.
- [31] R. Bondarescu, S. A. Teukolsky, and I. Wasserman, Phys. Rev. **D76**, 064019 (2007), 0704.0799.
- [32] W. C. Ho, N. Andersson, and B. Haskell, Phys.Rev.Lett. **107**, 101101 (2011), 1107.5064.
- [33] B. Haskell, N. Degenaar, and W. C. G. Ho, Mon. Not. Roy. Astron. Soc. **424**, 93 (2012), 1201.2101.
- [34] Virgo Collaboration, B. Abbott *et al.*, Astrophys.J. **713**, 671 (2010), 0909.3583.
- [35] B. J. Owen, Phys.Rev. **D82**, 104002 (2010), 1006.1994.
- [36] Q. D. Wang and E. V. Gotthelf, Astrophys. J. **494**, 623 (1998), arXiv:astro-ph/9708087.
- [37] A. G. Lyne, R. S. Pritchard, F. Graham-Smith, and F. Camilo, Nature (London) **381**, 497 (1996).
- [38] K. Thorne, Rev.Mod.Phys. **52**, 299 (1980).
- [39] LIGO Scientific Collaboration, B. Abbott *et al.*, Rept.Prog.Phys. **72**, 076901 (2009), 0711.3041.
- [40] A. Watts, B. Krishnan, L. Bildsten, and B. F. Schutz, Mon.Not.Roy.Astron.Soc. **389**, 839 (2008), 0803.4097.
- [41] M. Punturo *et al.*, Class.Quant.Grav. **27**, 194002 (2010).
- [42] K. S. Long *et al.*, Astrophys. J. **756**, 18 (2012), 1207.1555.
- [43] L. Lindblom, B. J. Owen, and G. Ushomirsky, Phys.Rev. **D62**, 084030 (2000), astro-ph/0006242.